Biogeosciences

Covariation of metabolic rates and cell size in coccolithophores

G. Aloisi

Laboratoire d'Océanographie et du Climat : Expérimentation et Approches Numériques, UMR7159,
CNRS-UPMC-IRD-MNHN, 75252 Paris, France

Correspondence to: G. Aloisi (galod@locean-ipsl.upmc.fr)

Abstract. Coccolithophores are sensitive recorders of environmental change. The size of their coccosphere varies in the ocean along gradients of environmental conditions and provides a key for understanding the fate of this important phytoplankton group in the future ocean. But interpreting field changes in coccosphere size in terms of laboratory observations is hard, mainly because the marine signal reflects the response of multiple morphotypes to changes in a combination of environmental variables. In this paper I examine the large corpus of published laboratory experiments with coccolithophores looking for relations between environmental conditions, metabolic rates and cell size (a proxy for coccosphere size). I show that growth, photosynthesis and, to a lesser extent, calcification covary with cell size when pCO_2, irradiance, temperature, nitrate, phosphate and iron conditions change. With the exception of phosphate and temperature, a change from limiting to non-limiting conditions always results in an increase in cell size. An increase in phosphate or temperature (below the optimum temperature for growth) produces the opposite effect. The magnitude of the coccosphere-size changes observed in the laboratory is comparable to that observed in the ocean. If the biological reasons behind the environment–metabolism–size link are understood, it will be possible to use coccosphere-size changes in the modern ocean and in marine sediments to investigate the fate of coccolithophores in the future ocean. This reasoning can be extended to the size of coccoliths if, as recent experiments are starting to show, coccolith size reacts to environmental change proportionally to coccosphere size. The coccolithophore database is strongly biased in favour of experiments with the coccolithophore *Emiliania huxleyi* (*E. huxleyi*; 82 % of database entries), and more experiments with other species are needed to understand whether these observations can be extended to coccolithophores in general.

I introduce a simple model that simulates the growth rate and the size of cells forced by nitrate and phosphate concentrations. By considering a simple rule that allocates the energy flow from nutrient acquisition to cell structure (biomass) and cell maturity (biological complexity, eventually leading to cell division), the model is able to reproduce the covariation of growth rate and cell size observed in laboratory experiments with *E. huxleyi* when these nutrients become limiting. These results support ongoing efforts to interpret coccosphere and coccolith size measurements in the context of climate change.

1 Introduction

Coccolithophores, the main calcifying phytoplankton group, are an important component of the oceanic carbon cycle (Broecker and Clark, 2009; Poulton et al., 2007). Through their cellular processes of photosynthesis (a CO_2 sink) and calcification (a source of CO_2), they contribute in defining the magnitude of the ocean–atmosphere CO_2 flux (Shutler et al., 2013). The calcium carbonate platelets (coccoliths) that make up their exoskeleton (coccosphere) provide ballast for dead organic matter in the photic zone, accelerating the export of carbon from the upper ocean to the sediments (Honjo et al., 2008). There is laboratory and field evidence that climate change is affecting the cellular processes and global distribution of coccolithophores, with potential consequences on the magnitude of the carbon fluxes introduced above (Gehlen et al., 2007; Wilson et al., 2012). For example, in laboratory cultures, the coccolithophore *E. huxleyi* shows reduced calcification-to-photosynthesis ratios when CO_2 is changed from pre-industrial levels to those predicted for the future, acidic ocean (Hoppe et al., 2011; Langer et al., 2009;

Riebesell et al., 2000; Zondervan et al., 2002). In the ocean, the coccolithophore *E. huxleyi* has been expanding polewards in the past 60 years, most likely driven by rising sea surface temperatures and the fertilizing effect of increased CO_2 levels (Winter et al., 2013). Despite the great number of laboratory experiments testing the effect of multiple environmental conditions on coccolithophore physiology (Iglesias-Rodriguez et al., 2008; Langer et al., 2012; Paasche et al., 1996; Riebesell et al., 2000; Riegman et al., 2000; Rouco et al., 2013; Sett et al., 2014; Zondervan, 2007; Zondervan et al., 2002), it is hard to link laboratory results with field observations to obtain a unified picture of how coccolithophores respond to changing environmental conditions (Poulton et al., 2014).

E. huxleyi is the most abundant, geographically distributed and studied coccolithophore (Iglesias-Rodríguez, 2002; Paasche, 2001; Winter et al., 2013). It exhibits a strong genetic diversity, with the different genotypes adapted to distinct environmental conditions (Cook et al., 2011; Iglesias-Rodríguez et al., 2006; Medlin et al., 1996) – a characteristic that explains its global distribution and ecological success in the modern ocean (Read et al., 2013). *E. huxleyi* morphotypes, which differ for their coccosphere size, as well as shape, size and degree of calcification of coccoliths (Young and Henriksen, 2003), correspond to at least three genetically distinct genotypes (Cook et al., 2011; Schroeder et al., 2005). The geographical distribution of *E. huxleyi* morphotypes in the ocean is controlled by environmental conditions (Beaufort et al., 2008, 2011; Cubillos et al., 2007; Henderiks et al., 2012; Poulton et al., 2011; Schiebel et al., 2011; Smith et al., 2012; Young et al., 2014). But the physiological role of key factors such as pCO_2 is controversial, with a study showing that high pCO_2 favours morphotypes with smaller and lighter coccoliths (Beaufort et al., 2011), and other studies showing the opposite (Grelaud et al., 2009; Iglesias-Rodriguez et al., 2008; Smith et al., 2012). Next to pCO_2, there is growing evidence that irradiance, nutrients and temperature also play a role in controlling morphotype biogeography (Berger et al., 2014; Henderiks et al., 2012; Smith et al., 2012). Despite the need for a better understanding, it is clear that the geographical distribution of *E. huxleyi* morphotypes carries precious information on how this key coccolithophore species will react to climate change.

But there is another, more subtle effect of climate change on coccolithophores: as living conditions evolve, cell size and coccosphere size adapt, due uniquely to a physiological response to environmental change. At the cellular scale, laboratory experiments with *E. huxleyi* show that pCO_2, irradiance, temperature and nutrient concentrations affect not only rates of photosynthesis and calcification but also cell and coccosphere size, without inducing a change in morphotype (Bach et al., 2011; De Bodt et al., 2010; Iglesias-Rodriguez et al., 2008; Muller et al., 2008; Müller et al., 2012; Oviedo et al., 2014; Rouco et al., 2013). Culture conditions also affect the size and mass of coccoliths (Bach et al., 2012; Boll-

mann and Herrle, 2007; Müller et al., 2012; Paasche et al., 1996; Satoh et al., 2008; Young and Westbroek, 1991). Coccolith size (length, volume) and weight are used as proxies for coccolithophore calcification because they are related to the total mass of calcite in the cell (Beaufort et al., 2011; although multiple layers of coccoliths around cells may complicate this simple picture). The size of coccoliths is positively related to that of coccospheres in laboratory experiments (Müller et al., 2012), in the ocean (Beaufort et al., 2008) and in marine sediments (Henderiks, 2008), and the mass of coccoliths is positively related to that of coccospheres in the ocean (Beaufort et al., 2011). These observations suggest that the physiological sensitivity of coccosphere and coccolith size to environmental conditions carries supplementary information on the reaction of *E. huxleyi* to climate change.

In the ocean, attempts have been made to disentangle the effect of multiple environmental parameters on the size and mass of *E. huxleyi* coccospheres and coccoliths (Beaufort et al., 2008, 2011; Cubillos et al., 2007; Hagino et al., 2005; Henderiks et al., 2012; Meier et al., 2014; Poulton et al., 2011; Young et al., 2014). This is a complicated task, primarily, as explained above, because changes in cell size are partly ecological in origin and some automatic measuring procedures do not distinguish between the different morphotypes (Beaufort et al., 2008, 2011; Meier et al., 2014) and, secondly, because environmental parameters covary in the field, making it hard to interpret size changes observed in the ocean in terms of those recorded in the laboratory. Nevertheless, a recent study based on scanning electron microscope observations suggests that the coccosphere size of *E. huxleyi* within a population of a given morphotype varies considerably and is likely under physiological control (Henderiks et al., 2012). Also, the size of coccoliths of a given morphotype varies in the modern ocean (Hagino et al., 2005; Henderiks et al., 2012; Poulton et al., 2011) as well as the recent geological past (Berger et al., 2014; Horigome et al., 2014), and is likely to be under the control of parameters other than pCO_2 (Horigome et al., 2014; Young et al., 2014). To take advantage of the physiological and environmental information carried by coccosphere and coccolith size, two steps need to be taken: first, the effect of single environmental parameters on coccosphere and coccolith size has to be systematically observed in the laboratory and, second, an understanding of the biological reasons behind cell-size changes needs to be developed.

In this paper I explore the available laboratory data of coccolithophore metabolic rates and cell size. The metabolic rates considered are the growth rate (in units of day^{-1}), the rate of photosynthesis (in units of $pgC\,cell^{-1}\,day^{-1}$) and the rate of calcification (in units of $pgC\,cell^{-1}\,day^{-1}$). First, I investigate how coccolithophore metabolic rates scale with cell size in five species of coccolithophores, and how this scaling compares to that of other phytoplankton groups. Second, I discuss how metabolic rates and coccosphere size of a

given coccolithophore species are affected by changes in environmental culture conditions. The laboratory changes in *E. huxleyi* coccosphere size are compared to coccosphere-size changes observed in the modern ocean across gradients of environmental change. Finally, I propose a simple model that explains why metabolic rates and cell size covary, with the hope that a few basic principles may be used in the future to extract environmental and metabolic information from coccosphere and coccolith measurements obtained in the field. This paper is based on a database of published results of culture experiments with coccolithophores – the next section introduces this database.

2 A database of coccolithophore metabolism and cell size

The database (Table 1, Appendix A1) is composed of data collected in 369 separate culture experiments with 28 strains belonging to five species of coccolithophores (*E. huxleyi*; *Gephyrocapsa oceanica*; *Calcidiscus leptoporus*; *Syracosphaera pulchra*; and *Coccolithus braarudii*, formerly known as *Coccolithus pelagicus*). These studies were carried out in batch reactors or chemostats, in a wide range of culture conditions, including variable irradiance, light cycle, temperature, nutrient concentration (NO_3, PO_4 and Fe) calcium and inorganic carbon concentrations (pCO_2, DIC, total alkalinity). The salinity and the concentration of magnesium are similar to that of seawater. The database reports measured values of growth rate μ, in units of day^{-1}; the particular organic (POC) and inorganic (PIC) carbon quota, in units of pgC cell^{-1}; and the cell-specific rates of photosynthesis (RPh) and calcification (RCa), in units of pgC cell^{-1} day^{-1}. These quantities are interrelated according to the following expressions:

$$\text{RPh} = \mu \times \text{POC} \tag{1}$$

and

$$\text{RCa} = \mu \times \text{PIC}. \tag{2}$$

Equations (1) and (2) were used to complete the database when only two out of three of growth rate, carbon content and cell-specific metabolic rates are presented in a given literature source. When possible, the DIC system data have been converted to the total pH scale so that pCO_2 can be compared across the data set. The database includes 120 measurements of coccosphere size carried out with Coulter counters, flow cytometers and optical and scanning electron microscopes (SEMs).

Some consideration of growth rate measurements in conditions of nutrient limitation is necessary. In nutrient-limited batch cultures, the growth rate decreases with time as nutrients are depleted, so that determining growth rates via cell counts yields erroneous results (Langer et al., 2013). Reliable growth rates in conditions of nutrient limitation can be obtained in chemostats, where the growth rate is controlled by setting the dilution rate of the medium and the cell population is continuously renovated (Langer et al., 2013). An alternative are semi-continuous cultures where cells are periodically harvested and inoculated into a new medium, allowing relatively constant growth conditions (LaRoche et al., 2010). When considering nutrient limitation, I thus chose to use only data produced in chemostat and semi-continuous culture experiments.

2.1 Normalized growth rates

The light cycle varies from experiment to experiment, ranging from continuous light to a 12 h–12 h light–dark cycle. In order to compare the growth rates from experiments with different light–dark cycles, the data need to be normalized with respect to the duration of the light period. Since photosynthesis is restricted to the light period, growth rates (μ, in day^{-1}) have been normalized to the length of the light period. This is done applying the following relationship (Rost et al., 2002):

$$\mu_i = \frac{\mu \times (L + D)}{L - D \times r}, \tag{3}$$

where μ_i (in day^{-1}) is the normalized, instantaneous growth rate; μ (in day^{-1}) is the growth rate measured via cell counts; L and D are the length (in hours) of the light and dark periods; and r, the factor which accounts for the respiratory loss of carbon during the dark period, is set to 0.15 (Laws and Bannister, 1980). Thus, the instantaneous growth rate μ_i, in units of day^{-1}, is the growth rate normalized to a light period of 24 h.

2.2 Normalized cell carbon quotas

The organic carbon quota (POC) is positively related to cell volume. To compare POC across the database, a large bias introduced by the sampling strategy needs to be considered. Specifically, in experiments with a light–dark cycle, POC increases during the day as small cells formed during nighttime division assimilate carbon and increase in size (Linschooten et al., 1991; Muller et al., 2008; Vanbleijswijk et al., 1994; Zondervan et al., 2002). Typically, sampling for POC measurements is carried out at different times during the light period in different experiments. This introduces variability in the POC data that is not related to the experimental growth conditions. When the time of sampling in the light cycle is reported, POC data have been normalized with respect to the time of sampling using the following equation (the derivation of this equation is given in Appendix A1):

$$\text{POC}(t) = \frac{L \cdot \text{POC}(S_T)}{L + S_T} \cdot \left(1 + \frac{t}{L}\right), \tag{4}$$

where L is the length (in hours) of the light period, S_T is the sampling time in hours after the beginning of the light period, $\text{POC}(S_T)$ is the POC measured in the experiment at

Table 1. Entries in the database of coccolithophore metabolism.

	Column content	Units/explanation
General information	Literature reference	–
	Coccolithophore species	Species name
	Coccolithophore strain	Strain name
	Experiment type	Batch or chemostat
	Optimal temperature of strain	°C
Experimental conditions	Duration light period	Hours
	Duration dark period	Hours
	Sampling time	Hours from beginning of light period
	Irradiance	$\mu mol\ photons\ m^{-2}\ s^{-1}$
	Temperature	°C
	Salinity	$g\ kg^{-1}$
	$p\mathrm{CO2}$	μatm
	Dissolved inorganic carbon (DIC)	$\mu mol\ kg^{-1}$
	pH_T (total scale)	pH units
	Total alkalinity (TA)	$\mu mol\ kg^{-1}$
	Saturation state (calcite)	–
	Ca	$mmol\ kg^{-1}$
	Mg	$mmol\ kg^{-1}$
	NO_3	$\mu mol\ kg^{-1}$
	PO_4	$\mu mol\ kg^{-1}$
Experimental results	Organic C quota (POC)	$pg_C\ cell^{-1}$
	Inorganic C quota (PIC)	$pg_C\ cell^{-1}$
	Growth rate	day^{-1}
	Photosynthesis rate (RPh)	$pgC\ cell^{-1}\ day^{-1}$
	Calcification rate (RCa)	$pgC\ cell^{-1}\ day^{-1}$
	Coccosphere diameter	μm

time S_T and t is the time at which the corrected POC value is calculated.

For experiments with a light–dark cycle where the sampling time is reported, I imposed $t = L/2$ in Eq. (4) to estimate the POC in the middle of the light phase. When the time of sampling is not reported, Eq. (4) was used to estimate a minimum and a maximum POC in the middle of the light phase assuming that the reported POC value was measured at the end and at the beginning of the light phase, respectively. This procedure was applied also to PIC values because inorganic carbon ($CaCO_3$) production takes place nearly exclusively during the light phase in coccolithophores (Muller et al., 2008) and PIC shows an evolution similar to POC during the light period (Zondervan et al., 2002). In experiments with continuous light the cell cycle is desynchronized such that the average cell diameter remains constant if environmental conditions do not change (Muller et al., 2008; Müller et al., 2012). Thus, the POC measurements were not corrected in these experiments. Interestingly, fossil coccolithophores represent an integrated sample over the whole light–dark cycle and thus should be more comparable to laboratory samples from desynchronizes cultures – something to keep in mind as the amount of morphological information of coccolithophores from marine sediments is growing (Beaufort et al., 2011; Grelaud et al., 2009).

2.3 Normalized cell-specific rates of photosynthesis and calcification

The normalized growth rates and normalized cell carbon quota are used to calculate normalized, cell-specific rates of photosynthesis (RPh$_i$, in $pgC\ cell^{-1}\ day^{-1}$) and calcification (RCa$_i$, in $pgC\ cell^{-1}\ day^{-1}$):

$$RPh_i = \mu_i \cdot POC_C, \tag{5}$$
$$RCa_i = \mu_i \cdot PIC_C. \tag{6}$$

Here the subscript C indicates that the carbon quota refers to the value in the middle of the light phase (calculated imposing $t = L/2$ in Eq. 4) and the subscript i indicates that the metabolic rates are normalized with respect to the light period (Eq. 3). Thus, RPh$_i$ and RCa$_i$ are the metabolic rates normalized to a light period of 24 h. When the time at which sampling occurred during the light period is not known, minimum and a maximum cell-specific rates of photosynthesis and calcification are calculated assuming that the reported

POC and PIC values were measured at the end and at the beginning of the light phase, respectively.

2.4 Estimating cell and coccosphere size from carbon quota

Coccosphere size data are reported only in a third of the experiments included in the data set (of which more than 80 % of measurements are for *E. huxleyi*), while no cell-size measurements are included in the database. To take advantage of the full set of metabolic measurements available, cell size and coccosphere size were estimated from the particulate organic (POC) and inorganic (PIC) carbon content per cell with the following expression (the full derivation is given in Appendix A2):

$$V_{\text{Sphere}} = \frac{1.8 \times \text{POC}}{d_{\text{POM}}} \cdot \left(1 + \frac{f_{\text{CY}}}{1 - f_{\text{CY}}}\right) + \frac{100}{12} \cdot \frac{\text{PIC}}{d_{\text{CaCO}_3}}$$
$$\cdot \left(1 + \frac{f_{\text{Sh}}}{1 - f_{\text{Sh}}}\right), \tag{7}$$

where V_{Sphere} is the volume of the coccosphere (Fig. 1) – the volume of the cell and shield are equal to the first and second term on the right in Eq. (7), respectively – d_{POM} (in g cm^{-3}) is the density of organic matter; d_{CaCO_3} (equal to 2.7 g cm^{-3}) is the density of CaCO_3; and f_{CY} and f_{Sh} are the volume fraction occupied by water in the cell and shield, respectively. Equation (7) assumes that cell volume scales linearly with cellular carbon content. This assumption is reasonable for coccolithophores due to the absence of large vacuoles (Paasche, 1967).

I used Eq. (7) to calculate the diameter of the cell and the coccosphere for all the experiments in the database for which POC and PIC data are available (Fig. 2). The unknowns in this equation are d_{POM}, f_{CY} and f_{SH}. First, d_{POM} was set to 1.5 g cm^{-3}, which lies at the centre of the range of values proposed by Walsby and Raynolds (1980; 1.3–1.7 g cm^{-3}). Then f_{CY} and f_{SH} were varied so that the resulting diameter of the great majority of *E. huxleyi* spheres fell in the range 3–7.5 μm, which approximately corresponds to the range reported in culture experiments (Fig. 2) and to that measured microscopically in surface waters off the coast of the Benguela upwelling system (Henderiks et al., 2012). The chosen values of f_{CY} (0.79) and f_{SH} (0.66) results in a difference between the diameter of the coccosphere and that of the cell of about 1.5 μm for most of *E. huxleyi* the cells (values significantly smaller or larger than 1.5 μm are interpreted in Appendix A2). This value, observed in cultures of *E. huxleyi* (Henderiks, personal communication, 2013), corresponds roughly to twice the thickness of one layer of coccoliths (and thus to one layer of coccoliths in the shield around one cell). This is consistent with the laboratory observation that most calcifying *E. huxleyi* cells regulate their calcification rates/division rates in order to maintain at least a complete layer of coccoliths, even in growth-limited conditions (Paasche, 1999). With these parameter settings, the resulting
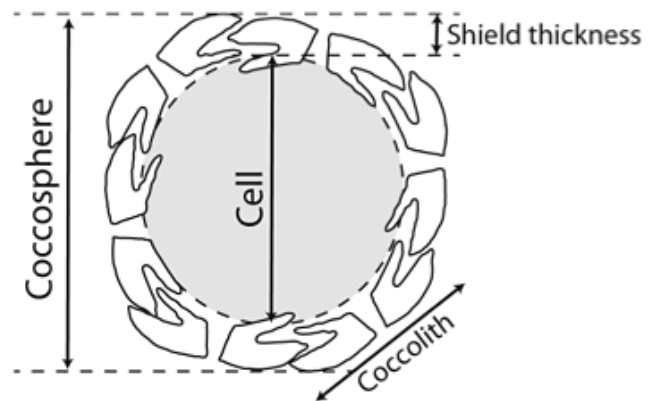

Figure 1. Schematic representation of a coccolithophore cell surrounded by a shield of coccoliths. The coccolith-bearing cell is called the coccosphere (modified from Hendericks, 2008).

density of the naked *E. huxleyi* cell is 0.18 pgC μm^{-3}, which is comparable to that of carbon in protist plankton of similar size determined by Menden-Deuer and Lessard (2000). The cell diameter obtained with this procedure is compared with that obtained applying an existing relation between POC and cell volume (Montagnes et al., 1994) in Appendix A1.

The calculated coccosphere diameter of *E. huxleyi* is compared to the measured coccosphere diameter for the experiments in the database where POC, PIC and cell-size data are reported (Fig. 2b). Although a clear positive relation between measured and calculated coccosphere size exists, the calculated diameters are always larger than the measured diameters (except for two experiments in Kaffes et al., 2010). The large majority of coccosphere-size measurements in the database were carried out with Coulter counters, which often do not include the coccolith shield in the size measurement (Iglesias-Rodriguez et al., 2008; Oviedo et al., 2014; van Rijssel and Gieskes, 2002). Consistently, the Coulter counter diameter for *E. huxleyi* corresponds to the cell diameter calculated with Eq. (7) (Fig. 2b). Another reason of the observed discrepancy is the fact that in some experiments cells are fixed chemically prior to size measurements, a treatment that induces cell shrinkage. Appendix A1 discusses the discrepancy between measured and calculated coccosphere size more in detail. With these considerations in mind, the choice made above of constraining Eq. (7) with the range of *E. huxleyi* coccosphere diameters measured with the microscope (Henderiks, 2008) appears to be the safest.

In Fig. 2c, the same parameterization of Eq. (7) is applied to the POC and PIC data available for the other coccolithophore species. A comparison with published coccosphere-size data for some of these species suggests that approach is reasonable. Most of the calculated coccosphere diameters for *Coccolithus braarudii*, for example, fall in the range 17–24 μm, which is slightly more extended than that reported by Henderiks (unpublished data reported graphi-

● *E. huxleyi*
◆ *G. oceanica*
■ *S. pulchra*
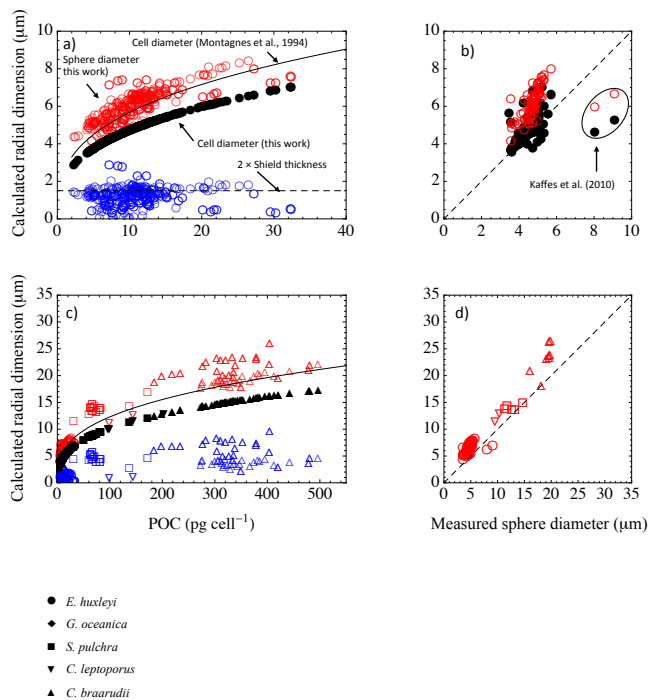▼ *C. leptoporus*
▲ *C. braarudii*

Figure 2. Geometric model used to obtain cell and coccosphere geometry from measurements of the particulate organic carbon (POC) and particulate inorganic carbon (PIC) content per cell measured in culture experiments. Panels **(a)** and **(c)** show the relationship between POC and PIC and cell geometry (cell and coccosphere diameter) calculated with Eq. (7). Panels **(b)** and **(d)** show the relationship between the cell and coccosphere diameter calculated with Eq. (7) and that measured in culture experiments. Notes: panels **(a)** and **(b)** present data for *E. huxleyi*, and panels **(c)** and **(d)** present data from the other coccolithophore species in the database. The filled black dots are the cell diameter, the empty red symbols are the coccosphere diameter and the empty blue symbols are the difference between the coccosphere and cell diameters.

cally in Fig. 7 of Henderiks, 2008; 18–22 μm). The corresponding shield thickness for *Coccolithus braarudii* falls into two groups (4.5 and 7.5 μm) suggesting the presence of more than one layer of coccoliths per cell in some cases. Similar to *E. huxleyi*, the coccosphere diameter measured with Coulter counters is always smaller than the calculated diameter (Fig. 2d). However, the discrepancy is small for these larger-sized species. Significantly, the coccosphere diameter of *Calcidiscus leptoporus* measured with SEM without prior fixing of cells by Langer et al. (2006) coincides with the calculated coccosphere diameter using Eq. (7) (Fig. 2d). When discussing cell and coccosphere size from experiments in the database I use Eq. (7) throughout the rest of this manuscript, regardless of whether size measurements are reported in the literature sources or not.

2.5 The allometric scaling of coccolithophore metabolism

In this section the coccolithophore database is used to investigate relationships between cell volume and metabolic rates across different taxa under comparable growth conditions (allometric relations). The differences in metabolic rates we will deal with are largely due to differences in characteristic cell size across different taxa. Allometric relationships for coccolithophores will be compared with similar relations for other phytoplankton groups compiled by Marañón (2008). The Marañón (2008) data set includes cell volume and metabolic rate data measured in the field for a vast array of unicellular photosynthetic organisms spanning 9 orders of magnitude in size, from photosynthetic cyanobacteria (volume $= 0.1\,\mu m^3$) to large diatoms (volume $= 10^8\,\mu m^3$) and including dinoflagellates and haptophytes. The Marañón (2008) data set reports rate measurements that mostly reflect in situ optimum growth conditions; thus, in this section, I focus on experiments in the coccolithophore database that were carried out in optimum conditions (Table 2). The assumptions made in comparing metabolic rates from the coccolithophore database with those measured in the field by Marañón (2008) are detailed in Appendix A2.

Figure 3a and b compare the allometric relations of photosynthesis and growth for coccolithophores with those established by Marañón (2008) for phytoplankton. Figure 3c and d show the allometric relations for photosynthesis and calcification in coccolithophores, highlighting the position of the five different coccolithophore species considered. Linear regressions through the optimum coccolithophore data set yield the following equations:

$$\log_{10}(\text{RPh}_i) = 0.89 \cdot \log_{10}(\text{Volume}) - 0.66, \tag{8}$$

$$\log_{10}(\mu_i) = -0.11 \cdot \log_{10}(\text{Volume}) + 0.1, \tag{9}$$

$$\log_{10}(\text{RCa}_i) = 1.02 \cdot \log_{10}(\text{Volume}) - 1.02. \tag{10}$$

The slope of the photosynthesis (0.89) and growth rate (−0.11) regressions for coccolithophores is very similar to that of the Marañón (2008) data set (0.91 and −0.09, respectively) and comparable to the slope of the regression through the calcification rate data (1.02). Furthermore, the different coccolithophore species occupy a position on the volume–photosynthesis diagram that is dictated by their cell size (Fig. 3c). These plots show that, for coccolithophores grown in optimum conditions, (1) photosynthesis in coccolithophores – including five different species spanning nearly 3 orders of magnitude in cell size – scales to cell volume in a comparable way as it does in other phytoplankton, (2) the size dependence of growth rates is very small for coccolithophores, and (3) calcification in optimum growth conditions scales isometrically with cell volume.

The finding of a near-isometric scaling of coccolithophore growth in laboratory experiments has implications for the

Table 2. Subgroups of experiments and the experimental conditions that define them.

Group name	n	Irradiance $\mu mol\, m^{-2}\, s^{-1}$	pCO_2 μatm	TA $mmol\, kg^{-1}$	PO_4 $\mu mol\, kg^{-1}$	NO_3 $\mu mol\, kg^{-1}$	Fe $nmol\, kg^{-1}$	Ca $mmol\, kg^{-1}$
Optimum low pCO_2	85	≥ 80	150–550	2.1–2.45	≥ 4	≥ 64	replete	9.3–10
Optimum high pCO_2	87	≥ 80	551–1311	1.9–2.6	≥ 4	≥ 64	replete	9.3–11.1
Light-limited	30	< 80	140–850	2.0–2.56	≥ 4	≥ 64	replete	9.3–10
NO_3-limited	10	≥ 80	200–1200*	2.3–4.5	≥ 4	limiting	replete	4–10
PO_4-limited	21	≥ 80	250–1200*	1–4.5	limiting	≥ 64	replete	4–10.6
Fe-limited	1	180	?	~ 2.35	4	64	limiting	10

*The DIC system data presented in the literature do not lend themselves to an accurate calculation of DIC system.
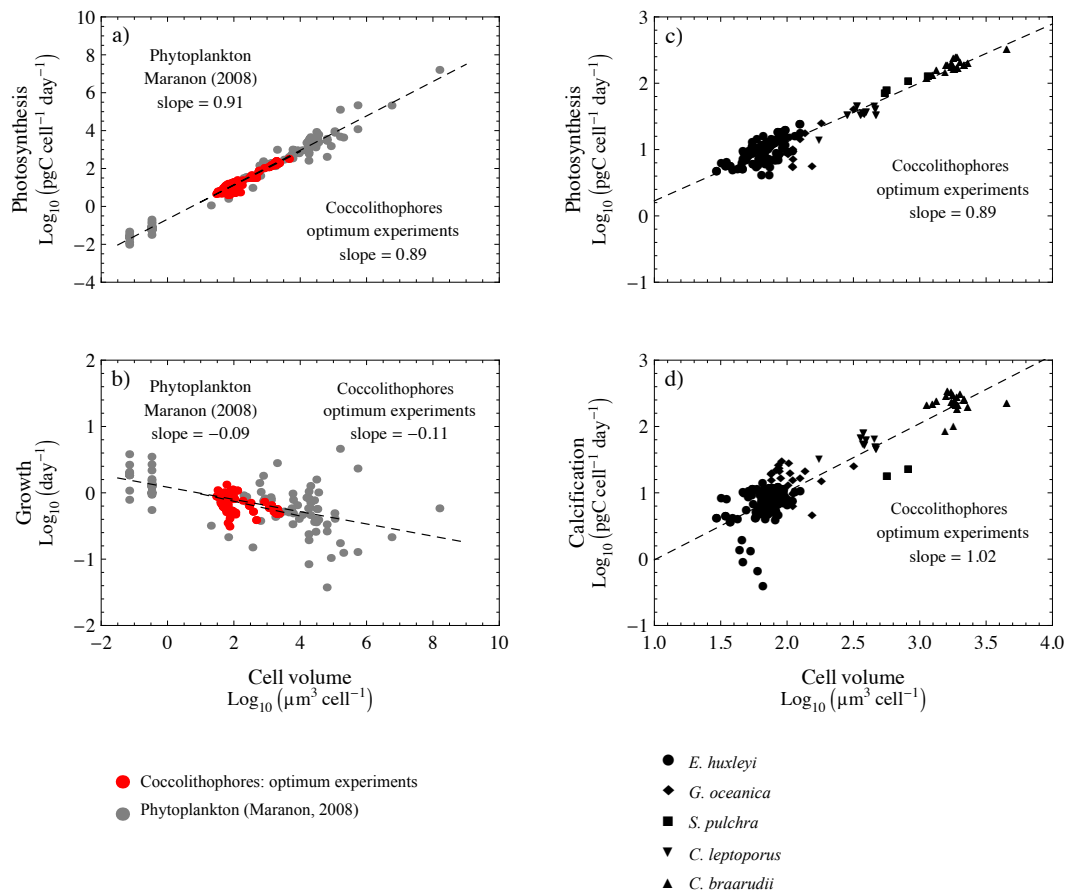

Figure 3. Allometric relationships between cell volume (Eq. 7) and photosynthesis rate (**a, c**; Eq. 5), growth rate (**b**; Eq. 3) and calcification rate (**d**; Eq. 6). Notes: in panels (**a**) and (**b**) red dots are the experiments from the coccolithophore database carried out in optimum growth conditions and grey dots are published field measurements of metabolic rates for a large number of organisms (Marañón, 2008); in panels (**c**) and (**d**) symbols denote coccolithophore species (see legend) and all data refer to optimum growth conditions. The dotted lines are the linear regressions through the experimental coccolithophore data obtained in optimum growth conditions and the field data of Marañón (2008; see Table 2 for definition of optimum growth conditions).

scaling of phytoplankton population abundance with body size in the ocean. In the ocean, including a variety of contrasting marine environments, phytoplankton population abundance scales with body size with an exponent equal to $-1/4$; in other words, small cells are more abundant than large cells

(Cermeño et al., 2006). Reviews of laboratory culture experiments with phytoplankton growth under optimal growth conditions suggest that cell-specific photosynthesis rates scale with cell volume with an exponent of 3/4 (Lopez-Urrutia et al., 2006; Niklas and Enquist, 2001), possibly a consequence

of the generic properties of transportation networks inside the organisms (Banavar et al., 2002; West et al., 1997). According to this scaling rule, growth rates scale with cell size with an exponent of $-1/4$, implying that large cells grow more slowly than small cells and offering an explanation for the size scaling of population abundance with cell size observed in the field (Cermeño et al., 2006).

However, the laboratory $-1/4$ scaling of growth rate to cell size has been challenged by the observation that the same scaling in natural communities of phytoplankton is nearly isometric (Huete-Ortega et al., 2012; Marañón, 2008; Marañón et al., 2007; i.e. a slope in Eq. (9) nearly equal to 0 and no effect of cell size on growth rate). The size exponent for different phytoplankton groups varies, with diatoms having a higher exponent (0.01) than that of dinoflagellates (-0.11; Marañón, 2008) and whole-community exponents varying from -0.01 (Marañón, 2008) to 0.16 (Huete-Ortega et al., 2012). An isometric scaling of growth rates to cell volume has recently also been observed in laboratory experiments with 22 species of phytoplankton ranging from 0.1 to $10^6 \, \mu m^3$ in volume (López-Sandoval et al., 2014; Marañón et al., 2013). In this context the coccolithophore data set is particularly relevant because it fills in the gap of sizes between 10^0 and $10^3 \, \mu m^3$ that is underrepresented in the Marañón (2008) data set. Furthermore, it confirms that a scaling exponent significantly smaller than $-1/4$ occurs in laboratory conditions, in addition to field situations, suggesting that cell size is not an important factor in determining the size distribution of coccolithophore populations. Taken together, the near-isometric scaling of growth rate with cell size observed in the ocean by Marañón (2008) and in the laboratory (López-Sandoval et al., 2014; Marañón et al., 2013) suggest that the $-3/4$ scaling of phytoplankton population abundance with cell size is not uniquely due to an effect of cell size on growth rates.

We are left with a contradiction that needs to be explained: whereas in some cases growth rates in the laboratory scale with cell size with an exponent of $-1/4$ (Lopez-Urrutia, 2006; Niklas and Enquist, 2001), this is not the case in the ocean (Huete-Ortega et al., 2012; Marañón, 2008; Marañón et al., 2007) and in some laboratory experiments (López-Sandoval et al., 2014; Marañón et al., 2013). With regard to laboratory experiments, López-Sandoval et al. (2014) point out that this difference could be in part due to the fact that older compilations of experimental data do not include cells smaller than $100 \, \mu m^3$. In the ocean, the larger phytoplankton (e.g. diatoms) have the ability to move vertically in the water column and adapt to variable nutrient and light conditions (Mitrovic et al., 2005; Stolte et al., 1994). This confers an advantage over small phytoplankton cells and provides a possible explanation for the near-isometric scaling of natural phytoplankton communities (Marañón, 2008). In laboratory experiments, where environmental parameters are typically constant, such extrinsic factors cannot be at play and some intrinsic, cellular-level property of coccolithophore cells must

exist that allows larger coccolithophores to overcome the geometrical constraints imposed by cell size on resource acquisition (Raven, 1998). Some coccolithophores posses carbon concentrating mechanisms (CCMs) that enable cells to take up HCO_3^-, as well as CO_2, for photosynthesis, and interconvert HCO_3^- to CO_2 internally via the carbonic anhydrate enzyme (Reinfelder, 2011; Rost et al., 2003). There is evidence from the carbon stable isotope composition of coccolithophore calcite that large coccolithophore species employ CCMs more efficiently than small species when CO_2 is scarce (Bolton and Stoll, 2013). This differential use of CCMs in large and small coccolithophore species offers a plausible (even if not exclusive) explanation of why coccolithophore growth rate scales nearly isometrically with cell size in laboratory experiments.

3   Environmental controls on cell size and metabolic rates in coccolithophores

In this section I investigate how changes in environmental conditions affect cell size and metabolic rates in coccolithophores. The changes we will deal with are produced by the physiological response of a given taxon to environmental change; I will discuss the effects of six environmental variables: pCO$_2$, irradiance, temperature, nitrate, phosphate and iron. Next to the optimum group of experiments introduced in Sect. 3, I highlight light-limited, nitrate-limited, phosphate-limited and iron-limited experiments. The set of conditions defining these groups is detailed in Table 2. Most of the data (82 % of database entries) come from cultures of *E. huxleyi*, the more thoroughly studied coccolithophore; experiments with the other four coccolithophores in the database have essentially tested the effect of pCO$_2$ conditions on growth, photosynthesis and calcification.

Within the optimum group of experiments, the position of the high-CO$_2$ subgroup largely corresponds to that of the low-pCO$_2$ group (Fig. 4). A considerable number of data points collected in suboptimal growth conditions, however, fall below the regression line through the optimal data. The scatter is greater for *E. huxleyi*, reflecting the fact that a much smaller number of environmental conditions have been tried out for the other species. For all rates of growth, photosynthesis and calcification, the light-limited experiments consistently plot below the optimum experiments (Fig. 4). The position of the nutrient-limited experiments below the optimum experiments is even more evident (Fig. 4): light-limited and nutrient-limited cells have smaller metabolic rates than cells of comparable size grown in optimum conditions. For experiments where the sampling time during the light period is unknown, the range of values for the photosynthetic rate (error bars) is large, and an overlap with an optimum group of experiments exists. However, only 5 out of 30 experiments in the light-limited group and 9 out of 31 nutrient-limited experiments have unknown sampling times, such that the po-

sition of the experiments run in limiting conditions under the optimum group of experiments is significant.

The plots of volume against metabolic rates introduced above do not take advantage of the whole potential of the experimental data set. This is because part of the variability in metabolic rates observed is due to differences in the pre-culture conditions and, very likely, to biological variability, rather than to the experimental conditions that the experiments are designed to test. A better picture is obtained if changes in cell volume are plotted against changes in metabolic rates. I have explored the database for sets of experiments where only one experimental condition is changed at a time, so that the change in volume and metabolic rates can be calculated by subtraction and plotted. In this way different sets of experiments can be compared on the same plot (this procedure is explained in detail in Appendix A3). The plots show the changes in metabolic rates and cell size induced by an increase in pCO_2; an increase in irradiance starting from light-limited conditions; an increase in temperature; and a decrease in nitrate, phosphate or iron starting from nutrient-replete conditions (Figs. 5 and 6). These changes correspond to the evolution of the living conditions that phytoplankton are experiencing (warming, acidification) or are expected to experience (ocean stratification leading to increased irradiance and oligotrophy) in the coming centuries (Behrenfeld et al., 2006; Bopp, 2005; Bopp et al., 2001). Tables 3 and 4 summarize the changes in cell and coccosphere diameter and volume induced by changes in experimental culture conditions. They highlight an important fact: changes in pCO_2 produce only limited variations in coccosphere size compared to variations in other parameters such as irradiance, temperature and nutrients.

3.1 pCO_2 increase

For the low-pCO_2 group of experiments run in optimum conditions (Fig. 5), an increase in pCO_2 leads to an increase in cell size and little change in the growth rate. The rate of photosynthesis increases with pCO_2, indicating that *E. huxleyi* is carbon-limited in this range of pCO_2. The biomass-specific calcification rate decreases in the great majority of the experiments, while the change in the rate of calcification can be positive or negative. Interestingly, the response of photosynthesis and calcification differ not only in sign, but also in homogeneity: while the change in photosynthetic rate defines a clear trend in the volume–metabolism space, the change in calcification rate is poorly correlated with the change in cell volume. This is not surprising given that the rate of photosynthesis increases both due to the fertilizing effect of CO_2 (physiological effect) and due to the increase in cell size (geometric effect), while the rate of calcification is positively affected by the increase in cell size (geometric effect) but inhibited physiologically by acidification (Raven and Crawfurd, 2012). This complex reaction of calcification to changes in the DIC system has been elegantly captured in a recent model

equation developed by Bach et al. (2015). Furthermore, the response of calcification to a rise in pCO_2 is modulated by the growth temperature (which varies between experiments) and can be negative or positive (Sett et al., 2014). Finally, the response of calcification in *E. huxleyi* to an increase in pCO_2 is known to be strain-specific, with a large span of responses possible (Langer et al., 2006). In all experiments but three, the ratio of calcification to photosynthesis decreases following the pCO_2 increase. Overall, the changes observed for the low-pCO_2 group of optimum experiments occur also in the high-pCO_2 group of experiments (albeit with a larger scatter) and in the experiments run in conditions of light limitation (Fig. 5). The few experiments available where pCO_2 is varied in conditions of nitrate limitation seem to point to a similar behaviour (see Appendix A3), as do the data available for other coccolithophore species (Fig. 5).

3.2   Irradiance increase in light-limited conditions

Increasing irradiance from irradiance-limited conditions leads to a large increase in cell size, growth rate and rate of photosynthesis (Fig. 6). In the majority of experiments the biomass-specific and cell-specific rates of calcification also increase with irradiance. The effects on the calcification-to-photosynthesis ratio are large, with most experiments showing an increase in calcification compared to photosynthesis. These effects are observed both in low-pCO_2 and high-pCO_2 conditions; they can be understood considering that both photosynthesis and calcification are light-dependent, energy-requiring processes (Brownlee et al., 1995; Raven and Crawfurd, 2012). Interestingly, there is a smaller dispersion in the calcification rate data compared to the set of experiments where pCO_2 is increased (Fig. 5). This is because both the geometric and physiological consequences of an irradiance increase concur in increasing the rate of calcification (geometric and physiological effects have contrasting influence on calcification rate for a pCO_2 rise). The experiments showing a negative response of the PIC / POC ratio with increased irradiance are from Rokitta and Rost (2012) and Feng et al. (2008), where high light intensities were used (300 and 400 μmol m^{-2} s^{-1}, respectively), possibly inducing photoinhibition of calcification (Feng et al., 2008).

3.3   Temperature

Both in optimum and light-limited conditions, an increase in temperature leads to an increase in the growth, photosynthesis and calcification rate and a decrease in cell size in the majority of the experiments considered (the scatter is considerable). This is consistent with the observation that *E. huxleyi* has the highest growth rate at temperatures 5–10 °C higher than the maxima observed at the isolation sites (Sett et al., 2014) – a pattern that seems to apply in general to phytoplankton from polar and temperate regions (Atkinson et al., 2003; Thomas et al., 2012). This trend has also been
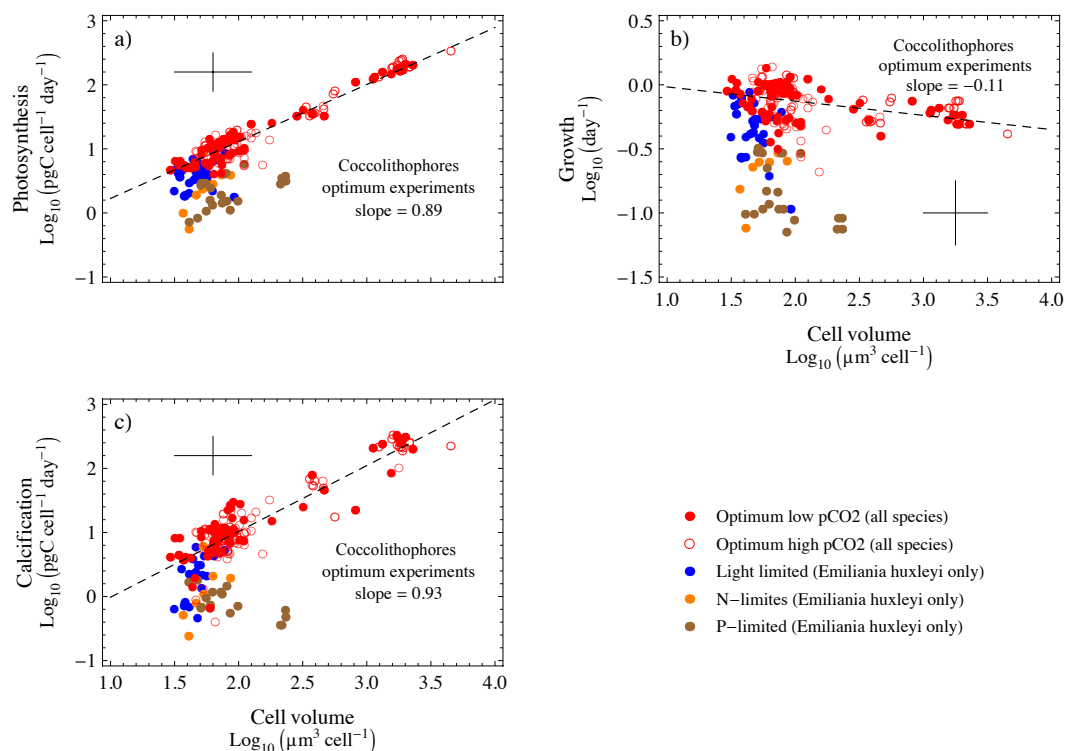
Figure 4. Effect of suboptimum growth conditions on allometric relationships for coccolithophores. **(a)** Rate of photosynthesis, **(b)** growth rate, and **(c)** rate of calcification. Suboptimum light and nutrient conditions result in cells having reduced metabolic rates compared to cells of equal size grown in optimal growth conditions (see Table 2 for definition of growth conditions). The error bars apply only to a limited number of experiments (see text) and correspond to those experiments where the sampling time is not reported.

Table 3. Changes in cell and coccosphere (sphere) volume for given changes in environmental conditions in culture experiments.

Condition changed	Mean value of environment change	Average cell (sphere) volume change (μm^3)	Average % cell volume (sphere) change	Max cell volume (sphere) change (μm^3)	Max % cell volume (sphere) change
pCO_2	$+209\,\mu atm$	$+8.6\,(+6.7)$	$+14.4\,(+5.2)$	$+23.5\,(+51.9)$	$+34.6\,(+36.6)$
pCO_2	$+592\,\mu atm$	$+12.6\,(+10.3)$	$+27.3\,(+12.8)$	$+63.4\,(+131.8)$	$+214.2\,(+185.6)$
Irradiance	$+193\,\mu E\,m^{-2}\,s^{-1}$	$+16.7\,(+39.5)$	$+38.0\,(+53.0)$	$+45.0\,(+93.0)$	$+120\,(+152.2)$
NO_3	Replete to limiting ($\sim 20\,nM$)	$-14.0\,(-33.0)$	$-22.2\,(-22.5)$	$-26.3\,(-80.0)$	$-33.1\,(-36.8)$
PO_4	Replete to limiting ($\sim 0.3\,nM$)	$+50.8\,(+73.5)$	$+43.8\,(+58.1)$	$+77.1\,(+93.6)$	$+67.8\,(+120.3)$
Fe	Replete to limiting	-32.2	-69.9	-32.2	-69.9
Temperature	$+7.6\,°C$ ($+5.8\,°C$)	-25.8 (-40.4)	-27 (-18.8)	-75.1 (-144.0)	-68 (-57.8)

described in an long-term experiment during which *E. huxleyi* was allowed to adapt for 1 year (roughly 460 asexual generations) to high temperatures (Schlüter et al., 2014).

3.4 NO₃, PO₄ and Fe limitation

Under nitrogen limitation, all cell-specific and biomass-specific metabolic rates decrease and cells become smaller (Fig. 6). The same effect on metabolic rates is observed under phosphorus limitation, but the effect on cell size is op-posite (Fig. 6). The contrasting effect of nitrogen and phosphorus limitation on cell size depends on the different role of these nutrient in the cell cycle (Muller et al., 2008). In the G1 (assimilation) phase of the cell cycle, nitrogen consumption by *E. huxleyi* cells is high because cells are synthesizing and accumulating biomass (Muller et al., 2008). Therefore, nitrogen depletion decreases assimilation rates and leads to smaller cells. The result is not dissimilar from what happens during light limitation. Phosphorous consumption, instead, is highest during the S and G2 + M phases, due to synthesis of

Table 4. Changes in cell and coccosphere (sphere) diameter for given changes in environmental conditions in culture experiments.

Condition changed	Mean value of environment change	Average cell diameter change (μm^3)	Average % cell (sphere) diameter change	Max cell (sphere) diameter (sphere) change (μm)	Max % cell (sphere) diameter change
pCO_2	+209 μatm	+0.2 (+0.1)	+4.5 (+1.6)	+0.5 (+0.7)	+10.4 (+11.0)
pCO_2	+592 μatm	+0.3 (+0.2)	+7.4 (+3.1)	+1.8 (+2.2)	+46.5 (+41.9)
Irradiance	+193 μE m^{-2} s^{-1}	+0.5 (+0.7)	+10.5 (+13.1)	+1.3 (+1.8)	+30.1 (+36.1)
NO$_3$	Replete to limiting ($\sim$ 20 nM)	−0.4 (−0.5)	−8.2 (−8.3)	−0.7 (−1.1)	−12.5 (−14.2)
PO$_4$	Replete to limiting ($\sim$ 0.3 nM)	+0.7 (+1.0)	+12.7 (+16.1)	+1.0 (+1.5)	+18.8 (+30.1)
Fe	Replete to limiting	−1.5	−33.3	−1.5	−33.3
Temperature	+7.6 °C (+5.8 °C)	−0.65 (−0.54)	−11.7 (−7.4)	−1.9 (−1.95)	−31.7 (−25)

nucleic acids and membrane phospholipids immediately before cell division (Geider and La Roche, 2002; Muller et al., 2008). Thus, phosphorus limitation is thought to arrest the cells in the G1 (assimilation) phase of the cell cycle, increasing the length of this phase and leading to an increase in the cell size. Thus, in phosphorus-limited cells, cell size does not increase because the assimilation rate increases but because the assimilation period is longer. The change in the ratio of photosynthesis to calcification is generally positive. In the only set of experiments considering iron limitation (Schulz et al., 2007), cell size covaries with growth and photosynthesis rates in a similar way as in nitrate-limited experiments (Fig. 6). Iron is a key component of CCMs that increase the rate of import of inorganic carbon (CO_2 and HCO_3^-) for photosynthesis, and of chlorophyll; thus, under iron-limiting conditions, the decrease in metabolic rates is produced by carbon limitation (Schulz et al., 2007). The concomitant decrease in cell size is consistent with the size shifts observed in the experiments where pCO_2 is varied (Fig. 5).

It should be noted that the coccolithophore database is strongly biased in favour of experiments with the coccolithophore *E. huxleyi* (82 % of database entries), and more experiments with other species are needed to understand whether the above relations between environment, cell size and metabolic rates can be extended to coccolithophores in general. Furthermore, the experiments included in the coccolithophore data set are designed to quantify the instantaneous (meaning a few generations) response of coccolithophores to changing growth conditions. In longer-term experiments, lasting several hundred generations (Lohbeck et al., 2012; Schlüter et al., 2014), *E. huxleyi* has been observed to adapt to elevated temperatures and pCO_2 conditions simulating future ocean conditions. This implies that the trends of metabolic rates and cell size with changing environmental conditions that are described in this section will be modulated by evolutionary adaptation, adding further complexity to the interpretation of past and future response of coccolithophores to climate change. The results of these experiments show, however, that the long-term response of growth rate and cell size to increased temperature and in-

creased pCO_2 are qualitatively comparable: cells adapted to high temperature decrease their cell size, while cells adapted to high pCO_2 increase their cell size (Schlüter et al., 2014).

4 The size of *E. huxleyi* in the ocean: is there hope of detecting a physiological signal?

In the previous section we saw that a change in laboratory culture conditions nearly always results in a change in cell and coccosphere size of coccolithophores. In this section the changes in coccosphere size observed in laboratory experiments are compared to those observed in the ocean. I will consider in some detail the BIOSOPE transect that crosses the South Pacific gyre from the Marquesas Islands to the Peru upwelling zone (Beaufort et al., 2008). Figure 7a shows the BIOSOPE transect superimposed on a surface ocean chlorophyll concentration map obtained from satellite observations. Figure 7b is a vertical transect in the upper 300 m of the ocean showing the variability in the diameter of coccospheres belonging to the order Isochrysidales. The order Isochrysidales is composed of the genera *Emiliania*, *Gephyrocapsa* and *Crenalithus*. These genera cannot be distinguished from one another by the automated SYRACO system used to measure coccosphere diameter and generate Fig. 7b. In addition to SYRACO, the BIOSOPE samples were examined with an SEM and a light microscope, which process less samples than SYRACO but are able to distinguish the different Isochrysidales genera.

Along the BIOSOPE transect the diameter and volume of Isochrysidales coccospheres measured with SYRACO varies considerably (from 4.5 to 8 μm Fig. 7b). SEM and light microscope observations show that between 140 and 130° W, where coccospheres are largest (mostly > 6 μm in diameter), *Gephyrocapsa oceanica* dominates the Isochrysidales assemblage (Beaufort et al., 2008). *Gephyrocapsa oceanica* has a characteristic cell size which is slightly larger than *E. huxleyi* (Fig. 3). In the Peru upwelling zone (75° W), where SYRACO detects large coccospheres (mostly > 6 μm in diameter), microscope observations show that *E. huxleyi* morphotype R, which is characteristically large ("overcalcified"),
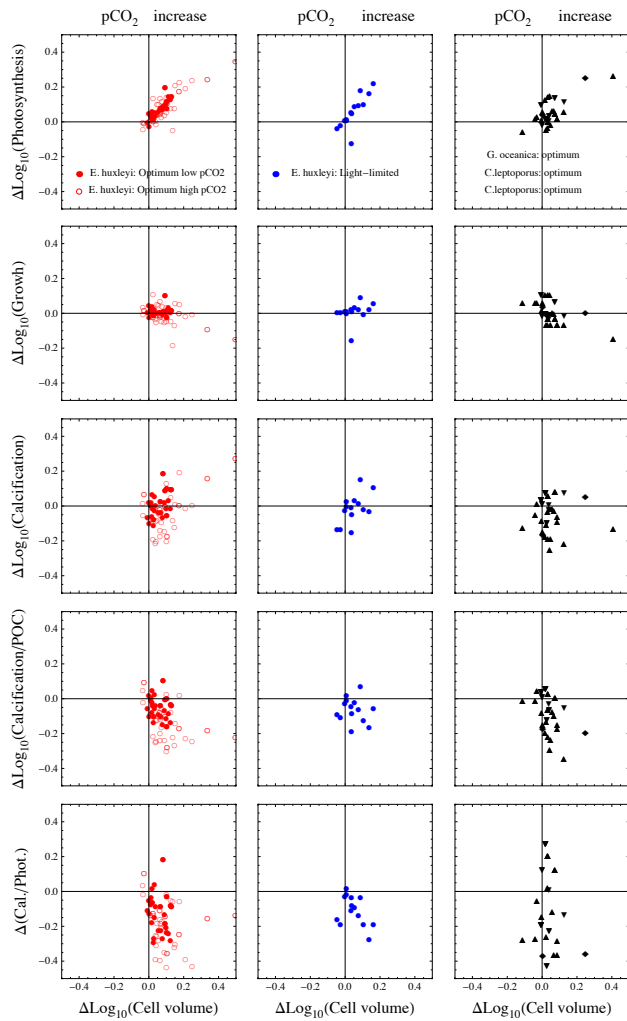
Figure 5. Changes in cell size and metabolic rates of *E. huxleyi* cells (first two columns) and other coccolithophore species (last column) subject to an increase in pCO_2. Note: for *E. huxleyi* symbols denote optimum low-pCO_2 conditions (red circles), optimum high-pCO_2 conditions (red dots), light-limited conditions (blue dots); for the other coccolithophore species symbols denote the species and all conditions are optimum, without distinction of pCO_2 range (see Table 2 for definition of growth conditions).

is abundant. Clearly, changes in coccosphere size along the BIOSOPE transect are partly ecological in origin – an observation that can be exported to the global ocean (Beaufort et al., 2011).

But how do the cell-size changes observed along the BIOSOPE transect compare with those observed in laboratory experiments? Whereas in the ocean changes in cell size can be due to both ecological and physiological effects, in the laboratory only physiological effects are expected. The histograms of Fig. 8a and b show the coccosphere diameter and volume of cultured *E. huxleyi* cells and of the Isochrysidales coccolithophores in the BIOSOPE transect. Labora-
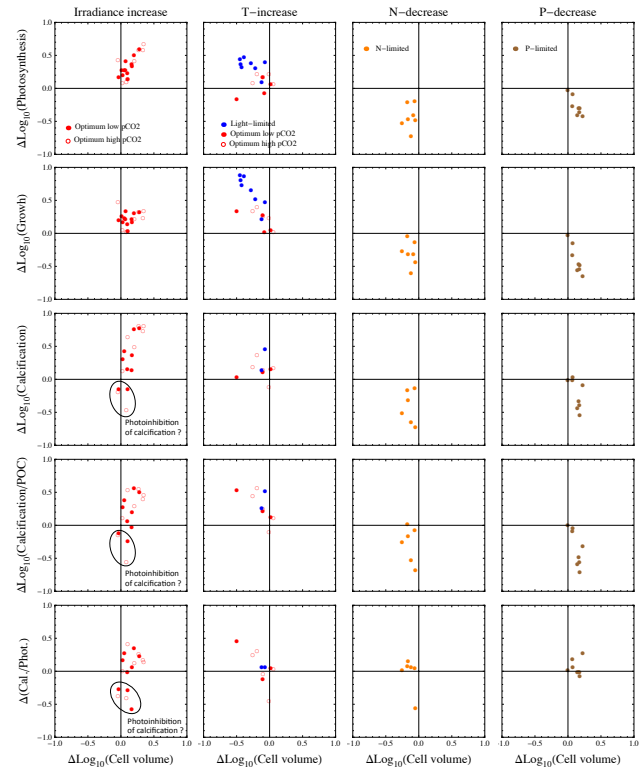

Figure 6. Changes in cell size and metabolic rates of *E. huxleyi* cells subject to an increase in irradiance (starting from irradiance-limited conditions), an increase in temperature and a decrease in nutrients (starting from nutrient-replete conditions). The symbols represent the different growth conditions defined in Table 2 except for iron, for which there is only one data point.

tory and field measurements compare well. The red horizontal bar graphs of Fig. 8a and b are the changes in coccosphere diameter and coccosphere volume observed in laboratory experiments for given variations in culture conditions (see also Tables 3 and 4). The comparison of histograms and bar charts shows that the variability in cell size in laboratory cultures is similar to that observed in the BIOSOPE transect. In Fig. 8c, the range of environmental conditions imposed in laboratory cultures is compared with the range of environmental conditions along the BIOSOPE transect. Large differences in the total range exist only for phosphate and iron, with concentrations in limited experiments being much lower than those measured in the BIOSOPE transect. Even with the phosphate and iron limitation experiments discarded, it is clear that changes in environmental conditions along the BIOSOPE transect are very likely to be an important driver of coccosphere-size variability: *physiological* effects concur with *ecological* effects in determining coccolithophore cell-size variability.

Further evidence for a physiological control on coccosphere size in the ocean comes from the Benguela coastal upwelling system, where the size of the well-calcified *E. huxleyi*
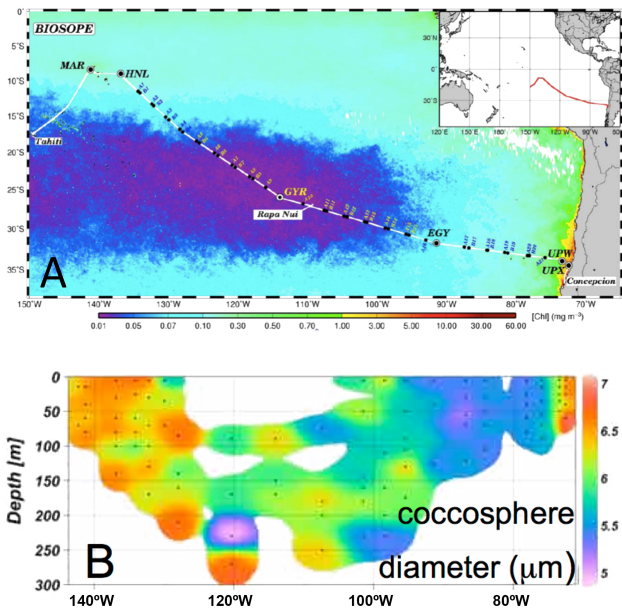
Figure 7. Geometry of Isochrysidales coccospheres along the BIOSOPE transect in the south-east Pacific ocean (Beaufort et al., 2008). **(a)** Geographical location of the BIOSOPE transect superimposed on the surface ocean chlorophyll concentration map obtained by satellite observations, and **(b)** distribution of Isochrysidales coccosphere diameter in depth along the BIOSOPE transect determined by the SYRACO automated coccolith analyser system (Beaufort et al., 2008).

morphotype A* (determined by SEM observations) changes considerably with environmental conditions (Henderiks et al., 2012). The largest coccospheres occurred at the depth of the deep chlorophyll maximum (DCM) – where growth conditions can be assumed to have been more favourable than in the overlying and underlying water masses – whereas coccospheres above and below the DCM were significantly smaller. This is consistent with the laboratory observations (Sect. 4) that environmental conditions which result in large growth rates (and thus lead to large populations in the field) are also those that give rise to large cells (phosphate concentrations in the Benguela upwelling system were much larger than those which induce an increase in cell size in culture experiments).

Another, even less explored (but equally promising) avenue of research is that of the physiological control of environmental conditions on the size of coccoliths. Field measurements of coccolith size are more abundant than measurements of coccosphere size. However, as for coccospheres, it is difficult to disentangle physiological from ecological effects. Clearly, different morphotypes occupy distinct ecological niches characterized by different environmental conditions. For example, Cubillos et al. (2007) show that type A ("overcalcified") and type B/C morphotypes occupy distinct latitudinal zones in the Southern Ocean. Environmental con-

ditions likely control the geographical distribution of different morphotypes on the east coast of Japan (Hagino et al., 2005), the Bay of Biscay (Smith et al., 2012), the Patagonian Shelf (Poulton et al., 2011) and the south-east Pacific (Beaufort et al., 2008). Clearly, part of the variability in coccolith size distribution in the global ocean is due to ecological effects (Beaufort et al., 2011).

There is laboratory and field evidence, however, that coccolith size is affected by environmental conditions also via physiological effects. Coccosphere and coccolith size are related (Henderiks, 2008). In laboratory cultures subject to varying pCO_2 and nitrate levels, coccolith volume (which is related to coccolith length) is positively correlated to both cell and coccosphere size (Müller et al., 2012), leading to the counterintuitive coexistence of large coccoliths and acidic conditions. An increase in the size of coccoliths with increasing pCO_2 has also been observed in nutrient-replete, nitrogen-limited and phosphate-limited experiments (Rouco et al., 2013). In the Benguela coastal upwelling system a significant positive correlation has been found between the coccosphere diameter and coccolith length of *E. huxleyi* morphotype A* (Henderiks et al., 2012). Since the Benguela correlation is based on SEM observations, it is likely that ecological effects can be excluded and that the physiological effects that produce larger coccospheres also result in the production of larger coccoliths. More generally, when the coccolith size from individual morphotypes is measured along gradients of environmental conditions, it results that coccolith size varies significantly – for example off the eastern coast of Japan (Hagino et al., 2005) and along the Patagonian shelf (Poulton et al., 2011). More experiments and field observations are needed to understand how other environmental parameters (e.g. temperature, irradiance and nutrient availability) affect coccolith size, and to what extent laboratory observations can be exported to the ocean. The available information suggests, however, that the environment controls coccolith size via a physiological effect and that there could be as much hidden information in the size of coccoliths as there is in the size of coccospheres. In the next section I propose a way to extract this information from the modern ocean and sedimentary record.

5 A theoretical basis for interpreting the covariation of metabolic rates and cell size

We saw that metabolic rates and cell size covary in coccolithophores subject to changes in laboratory environmental conditions (Sect. 4) and that the changes in coccosphere size observed in the laboratory are comparable in magnitude to those observed in the field along gradients of environmental change (Sect. 5). If the cellular processes that give rise to this covariation are understood, there is hope that coccosphere-size measurements from the field will yield information on the metabolic status of cells in the modern ocean and, pos-
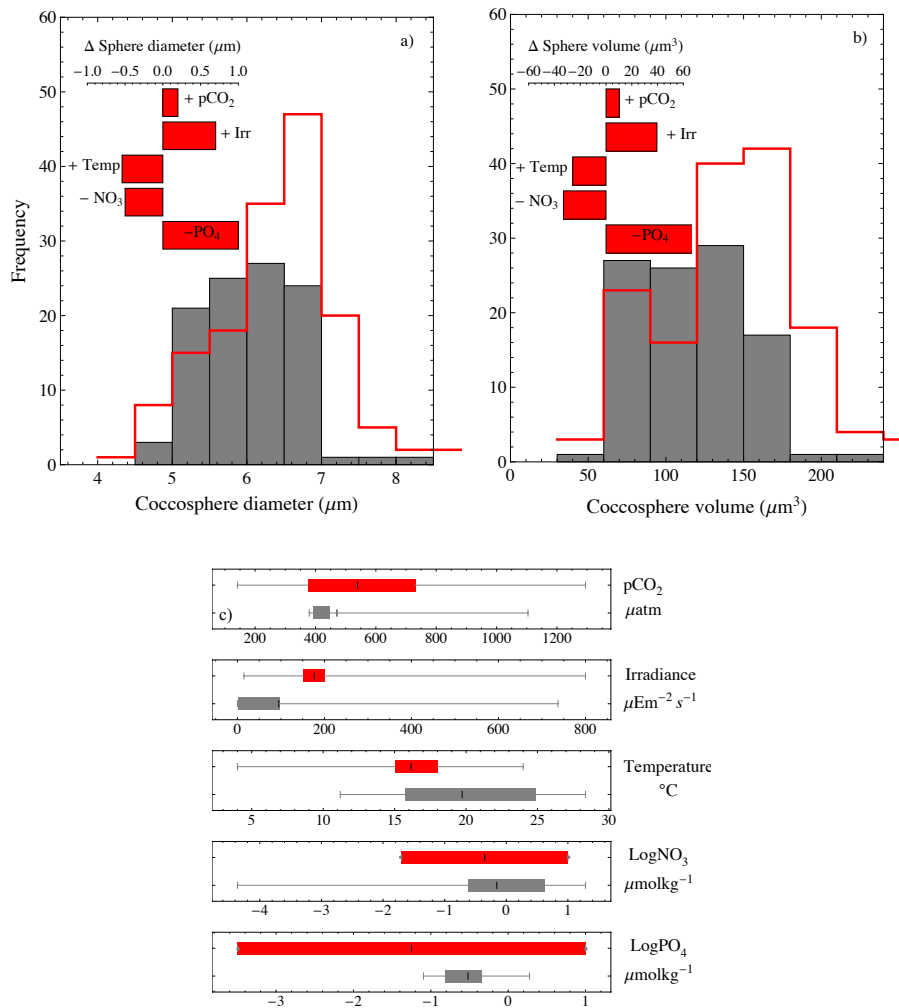
Figure 8. Comparison of the geometry (coccosphere diameter and volume) of Isochrysidales coccospheres from the BIOSOPE transect with the geometry of *E. huxleyi* coccospheres from laboratory culture experiments. Histograms in panels **(a)** and **(b)** compare BIOSOPE field data (grey) with experimental data (red). Horizontal bar graphs in panels **(a)** and **(b)** show the average changes in coccosphere geometry observed in *E. huxleyi* culture experiments for given changes in pCO$_2$, irradiance, temperature, NO$_3$ and PO$_4$. **(c)** Box-and-whisker plots comparing environmental conditions at the BIOSOPE stations where Isochrysidales coccosphere geometry measurements were made (grey) with the range of environmental conditions imposed in laboratory culture experiments with *E. huxleyi* (red). Box-and-whisker plots show the minimum value, lower quartile, median, upper quartile and maximum value of a given environmental parameter. Note: size data for Fe limitation is from one experiment in Schultz et al. (2007) and refers to cell size (not coccosphere size).

sibly, on past environmental conditions. In this section I introduce a simple model that provides a theoretical basis for understanding how cellular metabolism – forced by environmental conditions – controls cell size, giving rise to the correlations described in Sect. 4.

The mean size of dividing cells is the result of two factors: the rate of nutrient assimilation into biomass and the length of the generation time (the time between two successive cell divisions) – long generation times and large rates of nutrient assimilation give rise to large cells, and vice versa. The changes in cell size observed in the previous section can be interpreted within this simple scheme. The central concept I use – that of separation of structure (biomass) from maturity

(biological complexity, eventually leading to cell division) – is taken from the dynamic energy budget (DEB) theory (Kooijman, 2010). The model presented here is much simplified compared to existing DEB models of phytoplankton cells (Lorena et al., 2010; Muller et al., 2011; Muller and Nisbet, 2014). However, it considers the minimum number of concepts that are necessary to explain the covariance of metabolic rates and cell size we are dealing with. The most important simplifications I introduce are discussed in Appendix A4; the mathematical notation in this section follows that of Kooijman (2010).

Consider a spherical growing cell assimilating NO$_3$ and PO$_4$ (CO$_2$ is considered to be non-limiting). The assimilation
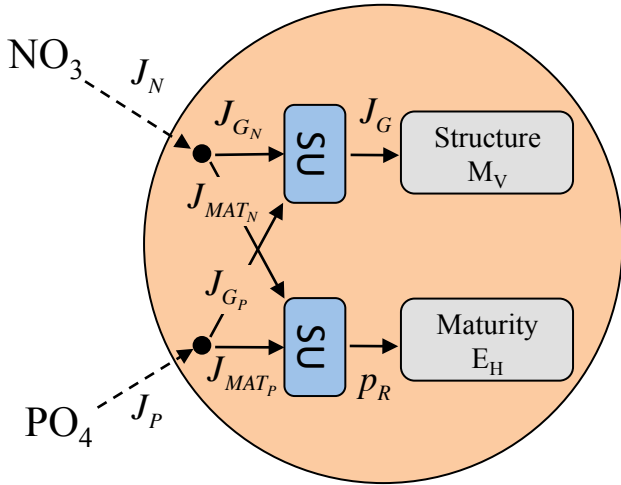
Figure 9. Simple physiological model of a dividing phytoplankton cell that reproduces the covariation of metabolic rates and cell size observed in coccolithophores. Notes: J_X – assimilation fluxes; J_{GX} – growth fluxes generated from the uptake of nutrient X; J_{MATX} – maturation fluxes generated from the uptake of nutrient X; J_G – total growth flux contributing to the build-up of structure (biomass) M_V; P_R – total maturation flux contributing to the build-up of maturity E_H; SU – synthesizing unit.

rate of nutrients, $\dot{j}_i$ (in µmol cell^{-1} day^{-1}), is proportional to the surface of the cell (Fig. 9):

$$\dot{j}_i = S \cdot j_{i\max} \cdot \frac{[i]}{[i] + K_i}, \qquad (11)$$

where the subscript i represents either NO$_3$ or PO$_4$, $\dot{j}_{i\max}$ (in µmol µm^{-2} day^{-1}) is the surface-specific maximum nutrient uptake rate, S (in µmol µm^{-2}) is cell surface, K_i (mol L^{-1}) is a Monod constant for nutrient uptake, and $[i]$ (in mol L^{-1}) is the nutrient concentration. Both the cell surface and the rate of nutrient assimilation are time-dependent because the model simulates a growing cell. Values of $\dot{j}_{i\max}$ were set equal to 4×10^{-9} and values of K_i were set equal to $0.2 \, \mu$mol L^{-1} and 2 nmol L^{-1} for NO$_3$ and PO$_4$, respectively, which is in the range of values determined for *E. huxleyi* (Riegman et al., 2000).

Assimilated nutrients are used to undertake two fundamental tasks (Fig. 9): (1) increase the cellular biomass via production of structure and (2) increase the maturity of the organism. In DEB theory the structure (quantified in moles of carbon per cell) contributes to the biomass of the organism (and thus cell volume) and is composed of organic compounds that have a long residence time in the cell. Maturity (quantified in joules per cell) has the formal status of information and is a measure of the complexity of the organism (Kooijman, 2010). Fundamental biological events in the lifespan of an organism, such as cell division, take place at a threshold level of maturity. Assimilated N and P both contribute to structure and maturity via the fluxes $\dot{j}_{G_i}$ and $\dot{j}_{MAT_i}$.

such that mass is conserved:

$$\dot{j}_{G_i} = \kappa \cdot \dot{j}_i \qquad (12)$$

and

$$\dot{j}_{MAT_i} = (1 - \kappa) \cdot \dot{j}_i, \qquad (13)$$

where κ, which takes a value from 0 to 1, is the portion of the nutrient uptake flux which is dedicated to growth, and $\dot{j}_{G_i}$ and $\dot{j}_{MAT_i}$ (in µmol$_i$ cell^{-1} day^{-1}) are the fluxes dedicated to growth and maturity, respectively. Dimensionless parameter κ was set equal to 0.5 both for NO$_3$ and for PO$_4$.

The growth fluxes generated from nutrient uptake, $\dot{j}_{G_i}$, are sent to a synthesizing unit (SU) for growth where biomass is synthesized at a rate $\dot{j}_G$ (in mol C cell^{-1} day^{-1}):

$$\dot{j}_G = 10^{-6} \cdot CN_{BIO} \cdot \left[\sum_{i=N,P} \left(\frac{\dot{j}_{G_i}}{y_{G_i}} \right)^{-1} - \left(\sum_{i=N,P} \frac{\dot{j}_{G_i}}{y_{G_i}} \right)^{-1} \right]^{-1}, \qquad (14)$$

where CN_{BIO} is the Redfield C / N ratio (equal to 106/16), necessary to transform the growth rate from units of mol N cell^{-1} day^{-1} to mol C cell^{-1} day^{-1}, and parameters y_{G_i} are the yield of nutrient flux i to the structure. The maturation fluxes generated from nutrient uptake, $\dot{j}_{MAT_i}$, are sent to another SU which tracks the build-up of maturity in the cell with a rate $\dot{p}_R$ (in joules cell^{-1} day^{-1}):

$$\dot{p}_R = 10^{-6} \cdot CN_{BIO} \cdot \mu_{MAT} \\ \cdot \left[\sum_{i=N,P} \left(\frac{\dot{j}_{MAT_i}}{y_{MAT_i}} \right)^{-1} - \left(\sum_{i=N,P} \frac{\dot{j}_{MAT_i}}{y_{MAT_i}} \right)^{-1} \right]^{-1} \qquad (15)$$

where μ_{MAT} (in joules mol C^{-1}) is the chemical potential of maturity (set equal to 10^5 joules mol C^{-1}) and the y_{MAT_i} are the yield of nutrient flux i to maturity. In this simple model, I set the yield parameters in Eqs. (14) and (15) such that NO$_3$ contributes primarily to the structure ($y_{G_{NO_3}} = 1$; $y_{G_{PO_4}} = 0.6$) and PO$_4$ to maturity ($y_{MAT_{NO_3}} = 0.6$; $y_{MAT_{PO_4}} = 1$).

The build-up of structure M_V (in mol C cell^{-1}) and maturity E_H (in joules cell^{-1}) is tracked by the following differential equations:

$$\frac{dM_V}{dt} = \dot{j}_G, \qquad (16)$$

$$\frac{dE_H}{dt} = \dot{p}_R. \qquad (17)$$

In DEB theory, volume, V (in µm^3), is obtained from the structural mass (the maturation flux is considered to dissipate in the environment and thus does not contribute to cell volume):

$$V = \frac{M_V \cdot \mu_V}{[E_G]}, \qquad (18)$$

where μ_V (joules mol C^{-1}) is the chemical potential of the structure and $[E_G]$ (in joules µm^{-3}) represents the volume-specific growth costs. In Eq. (18), the ratio of the chemical potential of the structure to the volume-specific growth costs can be obtained from the density of carbon in biomass, C$_{BIO}$, which is equal to 0.18 pg$_C$ µm^{-3} for *E. huxleyi* (Sect. 3):

$$\frac{\mu_V}{[E_G]} = 10^{12} \cdot \frac{m_C}{C_{BIO}}, \qquad (19)$$

where m_C ($= 12$) is the molecular weight of carbon and the factor 10^{12} is needed to convert pgC to gC. Thus, through substitution of the right-hand side of Eq. (19) into Eq. (18), the model calculates cell volume as follows:

$$V = \frac{M_V \cdot m_C \cdot 10^{12}}{C_{BIO}}. \qquad (20)$$

At any time, the instantaneous growth rate μ_{INST} (in day^{-1}) can be calculated as the ratio of the carbon uptake rate and the cellular carbon quota:

$$\mu_{INST} = \frac{j_G}{M_V}. \qquad (21)$$

Figure 10 shows how maturity, cell volume and the instantaneous growth rate (calculated with Eq. 21) evolve during a typical model run in non-limiting conditions. The model is run starting with initial cell size equal to 10 µm^3. As nutrients are taken up, they contribute to the structure. Biomass and cell size increase. As the cell grows, maturity accumulates until the threshold maturity for cell division is attained (dashed red line in Fig. 10a). The cell divides and a new cell cycle starts. After cell division the cell volume of the daughter cell is equal to half the volume of the parent cell, while the maturity buffer is emptied and the maturity of the daughter cell is set to zero. The instantaneous growth rate (Eq. 21) decreases during growth within a given cell cycle, consistent with the fact that the growth rate is proportional to the surface / volume ratio of cells. After a few cell cycles model variables (structure, maturity, volume etc.) repeat themselves from one cycle to another: the model has reached steady state. A full model run which brings the system into steady state lasts about 10 cell cycles. The final steady-state condition is independent of the initial cell size and depends only on nutrient concentrations and biological model parameters. The generation time is graphically visible as the horizontal distance between two successive division events. At steady state, the growth rate μ (in day^{-1}) can be approximated from the generation time G_T (in days; Powell, 1956):

$$\mu = \frac{\log 2}{G_T}. \qquad (22)$$

The growth rate calculated from the generation time (Eq. 22) is numerically equivalent to the average value of the instantaneous growth rate calculated with Eq. (21) (red dashed line
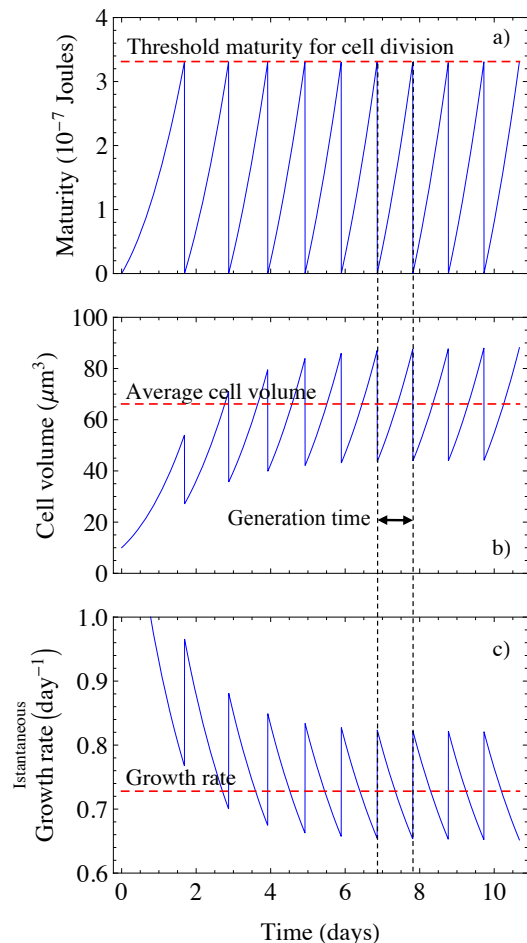

Figure 10. Evolution in time of modelled **(a)** maturity, **(b)** cell volume and **(c)** instantaneous growth rate of a cell undergoing 10 successive cycles of growth and division. Notes: the horizontal dashed line in **(a)** represents the threshold value of accumulated maturity in the cell at which cell division takes place, the horizontal dashed line in **(b)** is the average cell volume when cell cycles attain steady state, and the horizontal dashed line in **(c)** is the average instantaneous growth rate when cell cycles attain steady state and is numerically equivalent to the growth rate calculated from the generation time (vertical dashed lines) via Eq. (22) – it is conceptually equivalent to the growth rate measured from cell counts in culture experiments.

in Fig. 10c). In the following, I will discuss average cell volumes and growth rates at steady state (dashed red lines in Fig. 10b and c).

Next, the model is used to investigate how cell size and growth rate vary in conditions of nutrient limitation. The model is run changing NO$_3$ and PO$_4$ concentrations while keeping all the other model parameters unchanged. As explained above, the SUs were parameterized such that NO$_3$ contributes primarily to the structure (and to a lesser extent to maturity) and PO$_4$ contributes primarily to maturity (and to a lesser extent to the structure). The model was run 10 000 times with combinations of NO$_3$ and PO$_4$ concentra-
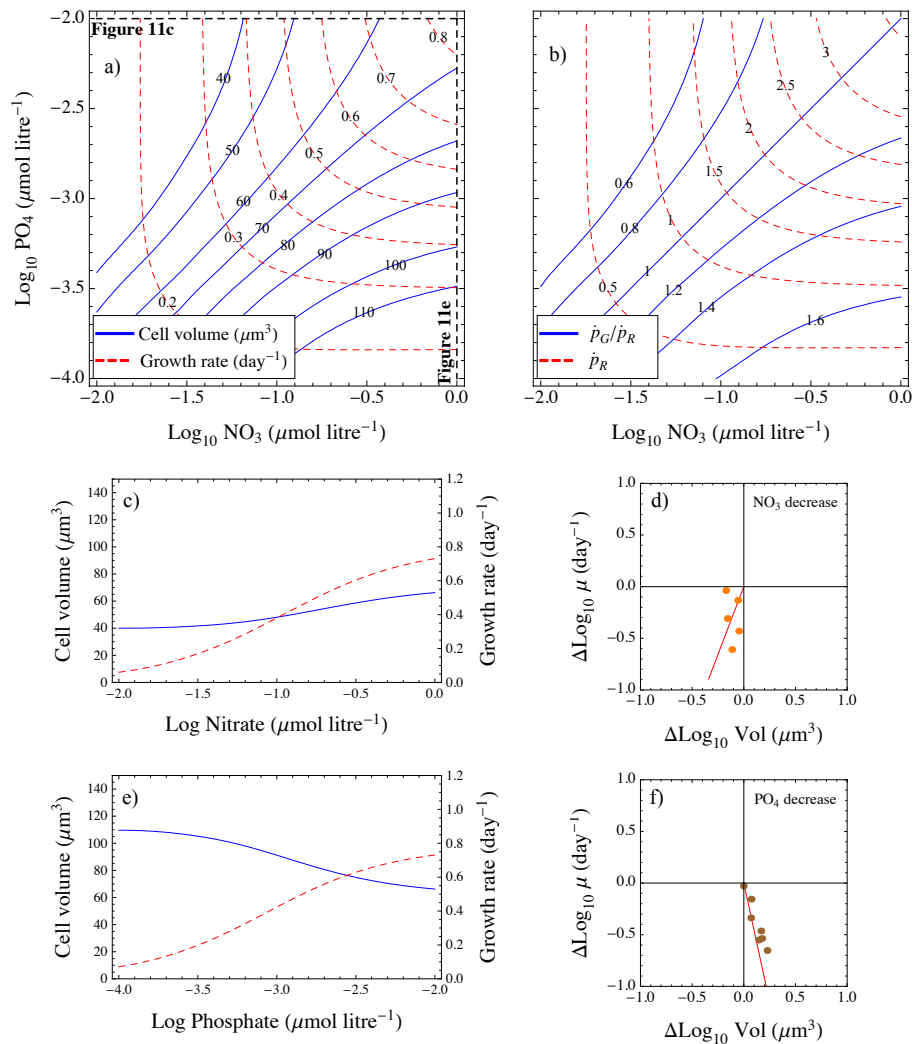
Figure 11. Effect of changing nitrate and phosphate concentrations on modelled cell volume and growth rate (**a**, **c**, **d**, **e** and **f**) and on the maturation flux P_R and the ratio of the growth to maturation fluxes P_G/P_R (**b**). Notes: the data points in (**d**) and (**f**) correspond to the shifts in cell size and growth rate observed in laboratory cultures with *E. huxleyi* subject to a decrease in nitrate (**d**) and phosphate (**f**) concentrations.

tions included between 10^{-2} to $1\,\mathrm{mmol\,L^{-1}}$ (NO$_3$) and 10^{-4} and $10^{-2}\,\mathrm{mmol\,L^{-1}}$ (PO$_4$; Fig. 11). Figure 11a shows how cell volume (blue contour lines) and growth rate (red dashed lines) depend on NO$_3$ and PO$_4$ concentrations: while NO$_3$ and PO$_4$ limitation both result in a decrease in the growth rate, they have contrasting effects on cell size, with NO$_3$ limitation resulting in a decrease size and PO$_4$ limitation in an increase in cell size. These trends are further displayed in Fig. 11b to e: Fig. 11b and c are plots of how growth rate and cell size vary when PO$_4$ is kept at non-limiting levels ($10^{-2}\,\mathrm{mmol\,L^{-1}}$) and NO$_3$ varies. Figure 11d and f are plots of how growth rate and cell size vary when NO$_3$ is kept at non-limiting levels ($1\,\mathrm{mmol\,L^{-1}}$) and PO$_4$ varies. Figure 11d and f are of the same sort as plots presented in Sect. 3, where changes in growth rate and cell volume induced by NO$_3$ and PO$_4$ limitation are represented on log scales. The experimen-

tal data from Riegman et al. (2000; orange points: NO$_3$ limitation; brown points: PO$_4$ limitation) are included in Fig. 11c and e.

These simulations show that the model can reproduce trends in growth rate and cell size observed in laboratory experiments when NO$_3$ and PO$_4$ become limiting (Sect. 5). In the following I discuss the features of the model that produce these trends. The growth rate is directly related to the generation time (Eq. 22). The generation time depends on the rate at which the maturity buffer is filled. Since both NO$_3$ and PO$_4$ contribute to the maturation flux, limitations in both NO$_3$ and PO$_4$ increase the generation time and a decrease in the growth rate. The link between growth rate and maturation flux is obvious if the maturation power is plotted as a function of NO$_3$ and PO$_4$ concentrations: the isolines of growth rate (Fig. 11a) follow those of the mat-

uration power (Fig. 11b). Controls on cell size are slightly more complicated. Cell size is affected both by the rate of biomass increase and by the generation time. Specifically, cell size is proportional both to the rate of biomass increase and to the generation time (and thus inversely proportional to the growth rate). The key model quantity determining how the average cell size changes following a change in nutrient concentrations is the ratio of the energy fluxes dedicated to growth and maturation:

$$\frac{\dot{p}_G}{\dot{p}_R}. \tag{23}$$

Figure 11b shows the value of this ratio as a function of NO_3 and PO_4 concentrations. On a diagonal line along which NO_3 and PO_4 decrease by proportionally the same amount, the growth / maturity ratio is constant and equal to 1 and cell volume does not change (Fig. 11a). If NO_3 decreases more than PO_4, then growth is more affected than maturity, leading to a decrease in cell size, and vice versa.

We conclude that changes in simple model quantities, which have a sound basis in biological metabolic theory, can explain the covariance of metabolic rates and cell size observed in laboratory experiments where nitrate and phosphate are limiting. Although the model was run with the uptake parameters of NO_3 and PO_4, the same trend of growth rate and cell size decrease with decreasing NO_3 concentrations is obtained if NO_3 is replaced by CO_2, or the Monod term for NO_3 is replaced by a Monod term for irradiance, suggesting that the simple set of rules discussed here can potentially explain the majority of the trends in metabolic rates and cell size described in Sect. 4. More work is needed to expand this simple physiological model to include other important features of full DEB models such as the distinction between reservoirs and structure, and to consider the interacting effect of multiple environmental changes. There is hope, however, that this effort will be rewarded by a better understanding of how environment affects the metabolic performance of coccolithophores in the modern ocean – a fundamental step in predicting how this important group of phytoplankton will be affected by climate change.

6 Conclusions

The examination of published results of coccolithophore culture experiments allows the following conclusions. The scaling of coccolithophore metabolism to cell size in optimal growth conditions is comparable to that observed in other phytoplankton groups by Marañón (2008). Larger taxa experience greater photosynthesis and calcification rates, while the growth rate is weakly dependent on cell size. In addition, cell size in *E. huxleyi* depends on environmental conditions. When only one of pCO_2, irradiance, temperature, NO_3, PO_4 or Fe is varied, cell size and metabolic rates covary, defining clear trends in the 2-D metabolism–cell-size space. An exception is calcification under variable pCO_2, which does not show clear trends. The magnitude of coccosphere-size changes observed by varying environmental culture conditions in the laboratory is comparable to the variability in *E. huxleyi* coccosphere size in the ocean. This suggests the existence of at least two controls on *E. huxleyi* cell size in the ocean: (1) the change in the relative abundance of *E. huxleyi* morphotypes with different characteristic cell sizes (*ecological* control) and (2) the change in coccosphere size induced by fluctuating environmental conditions (*physiological* control). Simple rules that regulate the partitioning of energy amongst growth and maturity explain the covariance of cell size and metabolic rates observed in laboratory experiments. There is hope that the dynamic energy budget theory – which formalizes this fundamental energy partitioning – can be used to interpret coccosphere and coccolith cell size in the past and modern ocean in terms of environmental change, providing a key for predicting the fate of coccolithophores in the future. In an evolutionary perspective, we can expect that adaptation to changing environmental conditions will modulate the observed metabolism–cell-size trends, adding further complexity in the study of past and future response of coccolithophores to climate change.

Appendix A: The coccolithophore database

The full coccolithophore database is presented in Table A1.

Normalized cell carbon quota

Due to cell division during the dark phase, POC at the end of the light phase (P_{END}) is double the POC at the beginning of the light phase (P_0):

$$POC_{END} = 2 \cdot POC_0. \tag{A1}$$

Thus, if POC increases linearly during the day, its evolution in time during the light phase can be expressed as follows:

$$POC(t) = POC_0 + \frac{t}{L} \cdot POC_0, \tag{A2}$$

where t is time in hours and L is the length of the light period in hours. To obtain an expression that calculates the carbon quota at any given time in the light phase, let S_T and $POC(S_T)$ be the sampling time and the corresponding POC value measured in an experiment. By substituting these values for $POC(t)$ and t in Eq. (A2) and rearranging, we can calculate POC_0:

$$POC_0 = \frac{L \cdot POC(S_T)}{L + S_T}. \tag{A3}$$

We can then substitute this expression for POC_0 in Eq. (A1) to obtain an expression calculating the POC at any time during the light period:

$$POC(t) = \frac{L \cdot POC(S_T)}{L + S_T} \cdot \left(1 + \frac{t}{L}\right). \tag{A4}$$

Estimating cell and coccosphere size from carbon quota

The volume of the coccosphere can be thought of as the volume of the cell (V_{Cell}) plus that of the coccolith shield (V_{Shield}; see Fig. 1):

$$V_{Sphere} = V_{Cell} + V_{Shield}. \tag{A5}$$

Both the cell and the shield contain water. Therefore, the volume of the cell can be expressed as

$$V_{Cell} = V_{POM} + V_{H_2OCell}, \tag{A6}$$

where V_{POM} is the volume occupied by organic matter and V_{H_2OCell} is the volume occupied by water in the cell. Similarly, the volume of the shield can be expressed as

$$V_{Shield} = V_{CaCO_3} + V_{H_2OShield}, \tag{A7}$$

where V_{CaCO_3} is the volume of the $CaCO_3$ in all the coccoliths of the shield and $V_{H_2OShield}$ is the volume of water contained in the shield. Defining f_{CY} and f_{SH} as the volume fractions of water in the cell and shield, respectively, the volume of the coccosphere can be expressed as

$$V_{Sphere} = V_{POM} + \frac{f_{CY}}{1 - f_{CY}} \cdot V_{POM} + V_{CaCO_3}$$
$$+ \frac{f_{Sh}}{1 - f_{Sh}} \cdot V_{CaCO_3}. \tag{A8}$$

Expressing volumes in terms of mass divided by density, the above equation becomes

$$V_{Sphere} = \frac{M_{POM}}{d_{POM}} \cdot \left(1 + \frac{f_{CY}}{1 - f_{CY}}\right) + \frac{M_{CaCO_3}}{d_{CaCO_3}}$$
$$\cdot \left(1 + \frac{f_{Sh}}{1 - f_{Sh}}\right), \tag{A9}$$

where M_{POM} and M_{CaCO_3} are the mass of organic matter and $CaCO_3$ in the coccosphere, respectively, and d_{POM} (1.3–1.7 g cm^{-3}; Walsby and Raynolds, 1980) and d_{CaCO_3} (2.7 g cm^{-3}) are the density of organic matter and $CaCO_3$, respectively. M_{POM} is related to the organic carbon per cell (POC; Muller et al., 1986),

$$M_{POM} = 1.8 \cdot POC, \tag{A10}$$

while the total mass of the coccoliths is related to the inorganic carbon content (PIC) per cell by

$$M_{CaCO_3} = \frac{MW_{CaCO_3}}{MW_C} \cdot PIC, \tag{A11}$$

where MW_C is the molecular weight of carbon (12) and MW_{CaCO_3} is the molecular weight of $CaCO_3$ (100).

Substituting Eqs. (A10) and (A11) in Eq. (A9), the volume of the coccosphere can be expressed as

$$V_{Sphere} = \frac{1.8 \cdot POC}{d_{POM}} \cdot \left(1 + \frac{f_{CY}}{1 - f_{CY}}\right) + \frac{100}{12} \cdot \frac{PIC}{d_{CaCO_3}}$$
$$\cdot \left(1 + \frac{f_{Sh}}{1 - f_{Sh}}\right). \tag{A12}$$

As explained in Sect. 2.4, the values chosen for f_{CY} (0.79) and f_{SH} (0.66) results in a difference between the diameter of the coccosphere and that of the cell of about 1.5 µm for most of the *E. huxleyi* cells. Values significantly smaller than 1.5 are observed when cells are cultured in Ca^{2+}-poor fluids (Riegman et al., 2000; Trimborn et al., 2007), low saturation states or undersaturation with respect to $CaCO_3$ (Bach et al., 2011; Borchard et al., 2011), or at very low light irradiances of 15 and 30 µmol photons m^2 s^{-1} in (Zondervan et al., 2002). In the case of Feng et al. (2008), small values of the coccosphere–cell diameter difference occur at high irradiances (400 µmol photons m^2 s^{-1}) and are interpreted as reflecting inhibition of calcification at high irradiance. In three of the experiments carried out by De Bodt et al. (2010), the coccosphere–cell diameter difference is roughly double

($\sim 3\,\mu$m), suggesting the presence of two layers of coccoliths making up the shield that surrounds the cell.

The reconstruction of cell geometry obtained by applying Eq. (7) is compared to that obtained applying the equation of Montagnes et al. (1994) which relates cell carbon content (C, in pg cell^{-1}) to cell volume (V, in μm^3):

$$C = 0.109 \cdot V^{0.991}. \tag{A13}$$

The diameter of *E. huxleyi* cells calculated with this formula is shown in Fig. 2a. The resulting cell diameter is up to $1.5\,\mu$m larger than that obtained with Eq. (7). I decided to use Eq. (7), rather than the equation of Montagnes et al. (1994), because the equation of Montagnes et al. (1994) implies a much lower density of carbon per cell (0.1 pgC μm^{-3}) and would result in *E. huxleyi* spheres larger (up to $12\,\mu$m diameter) than those observed in culture and in the field. Similar to *E. huxleyi*, if the relation between cell volume and carbon quota per cell of Montagnes et al. (1994; Eq. A13) is applied to the *Coccolithus braarudii* POC data, then the resulting coccosphere diameters for most of the coccospheres in the database (20–25 μm) are higher than those reported in Henderiks (Henderiks, 2008; 18–22 μm; Fig. 2c).

Figure 2 shows that the measured coccosphere diameter is always smaller than the coccosphere diameter calculated with the geometric model (Eq. 7). The large majority of coccosphere-size measurements in the database were carried out with Coulter counters (Table A2). It is known that cell-size measurements obtained with the Coulter counter underestimates the real coccosphere size as measured by SEM, possibly because the Coulter counter does not see the coccolith shield (Oviedo et al., 2014). Iglesias-Rodriguez et al. (2008) also report coccosphere-size measurements obtained with Coulter counters that are significantly smaller those obtained with flow cytometry. In fact, their Coulter counter measurements are very similar to the flow cytometer measurements after acidification of the sample, consistent with the idea that the Coulter counter does not see the coccolith shield (Oviedo et al., 2014). Similarly, by comparing light microscope measurements with Coulter counter measurements, van Rijssel and Gieskes (2002) report that the Coulter counter does not see the coccosphere. These considerations seem to be confirmed by the experiments of Langer et al. (2006) with *Calcidiscus leptoporus*, for which the coccosphere volume determined with Eq. (7) coincides with the SEM-derived volume (without prior fixing of the cells).

Appendix B: Comparing the coccolithophore database with the Marañón (2008) phytoplankton database

Marañón (2008) reports metabolic rate measurements carried out in the field (via cell counts and ^{14}C radiolabelling during incubation experiments lasting a maximum of approximately 1 day) that are as far as possible representative of in situ rates. Further, he chose to plot data for organisms growing in conditions of irradiance and nutrient availability that were more favourable for growth, and ran incubations at in situ temperature. However, nutrient limitation and suboptimal irradiance conditions cannot be excluded for some of the measurements included in his review (Marañón, personal communication, 2015). In his compilation, the photosynthetic rates reported in units of $pgC\,cell^{-1}\,h^{-1}$ are converted in $pgC\,cell^{-1}\,day^{-1}$ by multiplying by the length of the photoperiod that may be different for different locations. When the length of the photoperiod was not available, Marañón (2008) used a photoperiod of 12 h (Marañón, personal communication, 2014). In comparing the data of my data set with the data of Marañón (2008), I divided the instantaneous growth rate (μ_i) and cell-specific metabolic rates (RPh_i and RCa_i) obtained with Eqs. (5) and (6) by 2, obtaining rates that refer to a photoperiod of 12 h. Furthermore, I concentrate on the experiments from the coccolithophore database that were carried out in culture conditions that presumably do not depart too much from those of Marañón (2008). I thus selected 172 "optimum experiments" (Table 2) carried out in conditions of high irradiance ($\geq$ than $80\,\mu mol\,photons\,m^2\,s^{-1}$), nutrient-replete conditions (dissolved PO_4 and $NO_3 \geq 4$ and $64\,\mu M$, respectively) and dissolved Ca between 9 and 11.3 mM. I further subdivided these optimum experiments into a "low-pCO_2" subgroup, with pCO_2 included between 150 and $550\,\mu atm$ and total alkalinity between 2.1 and $2.45\,mol\,kg^{-1}$, and a "high-pCO_2" subgroup, with pCO_2 included between 551 and $1311\,\mu atm$ and total alkalinity between 1.9 and $2.6\,mol\,kg^{-1}$. The low-pCO_2 subgroup is representative of the ranges of the monthly means values of pCO_2 and total alkalinity in the surface ocean (Lee et al., 2006; Takahashi, 2009). No distinction between low-pCO_2 and high-pCO_2 subgroups is made in Sect. 3, where both groups are collectively referred to as the "optimum" group. Instead, the low-pCO_2 and high-pCO_2 subgroups are discussed separately and have distinct symbols in the plots of Sects. 4 and 5.

Table B1. Summary of methods used to determine the size of coccospheres in experiments included in the coccolithophore database.

	Measurement type	Fixation reported	Notes
Müller et al. (2012)	CC[a]	no	Reports difference between non-acidified and acidified samples
Lefebvre et al. (2011)	FC[b]	no	
Borchard et al. (2011)	CC	no	
Bach et al. (2011)	CC	no	
Krug et al. (2011)	?	no	
Kaffes et al. (2010)	CC	no	
Fiorini et al. (2011)	CC	no	
De Bodt et al. (2010)	CC	yes	
Iglesias-Rodriguez et al. (2008)	CC and FC	yes, both	Coulter size $\ll$ cytometer size. Coulter $=$ cytometer after acidification
Langer et al. (2006)	SEM[c]	no	SEM-measured size coincides with size calculated with Eq. (7)
Sciandra et al. (2003)	HOPC[d] and CC	no	HOPC results similar to CC results
Riegman et al. (2000)	CC	no	
van Rijssel and Gieskes (2002)	CC and LM[e]	no	LM measurement shows that coccosphere is not included in CC measurement
Arnold et al. (2013)	CC	no	

[a] Coulter counter, [b] flow cytometer, [c] SEM, [d] HIAC optical particle counter, [e] light microscope.

Appendix C: Comparison of changes in cell size with changes in metabolic rates

Method

In Sect. 4 the changes in cell size and metabolic rates induced by a shift in a given environmental parameter are discussed. For example, with regards to variations in pCO_2, I singled out groups of culture experiments where pCO_2 was the only environmental parameter that varied, while all other culture and pre-culture conditions were reported to be constant. For every such group of experiments I recorded the difference in cell volume and metabolic rates between cells grown at a given pCO_2 and those of the experiment carried out at the lowest pCO_2 level. For example, Langer et al. (2009) carried out four experiments with *E. huxleyi* clone RCC 1238 at pCO_2 levels of 218, 412, 697 and 943 µatm. Except for the DIC parameters that covary with pCO_2, all other pre-culture and experimental conditions were the same. For this group of four experiments I calculated the difference in cell volume and metabolic rates between the experiments at 412, 697 and 943 µatm and the experiment at 218 µatm, obtaining the displacement in the 2-D volume–metabolism space for the three experiments carried out at 412, 697 and 943 µatm.

Irradiance and temperature changes

Ideally, when comparing experiments at different irradiance and temperature levels, all other experimental parameters should be constant. In the Zondervan et al. (2002) experiments I selected couples of experiments with different irradiance and similar DIC system parameters. Similarly, I compared experiments at different temperature but similar pCO_2 conditions in the set of experiments by Sett et al. (2014). The difference in pCO_2 between different irradiance or temperature conditions was never greater than 150 µatm. Given the effect of pCO_2 on cell size and metabolic rates (Fig. 5), some of the variability shown in the plots that show how metabolic rates covary with cell size when irradiance or temperature increases (Fig. 6) will be due to variations in pCO_2.

Nutrient limitation

In Müller et al. (2012) the evolution in the 2-D volume–metabolism space is obtained by comparing nitrate-replete, batch and nitrate-limited chemostat experiments with comparable DIC systems. In this way the only aquatic chemistry difference is in the dissolved nitrate concentration. In the N-limited chemostat experiments of Riegman et al. (2000), the displacement in the 2-D size–metabolism space is obtained by the difference between the highest growth rate (0.61 day^{-1}) and the nitrate-limited experiments that have lower growth rates (0.15 to 0.45 day^{-1}). In the semi-continuous cultures of Kaffes et al. (2010) the data obtained in NO$_3$-replete conditions ($\sim$ 280 µM) were compared with that obtained at "ambient" (North Atlantic) NO$_3$ con-

centrations ($\sim$ 10 µM). Similar to the nitrate-limited experiments of Riegman et al. (2000), in the P-limited experiment of Borchard et al. (2011) and Riegman et al. (2000), the displacement in the size–metabolism space is obtained by the difference of size and metabolism at the different dilution rates (which have different dissolved P concentrations).

The shift in cell size, growth and photosynthesis rate produced by iron limitation is deduced from the experiments of Schultz et al. (2007). These are batch experiments, so the growth rates estimated from cell counts are not reliable (Langer et al., 2013). Nevertheless, the iron-limited experiment was included because the batch experiments inform on the direction of change (positive or negative) of cell size and metabolic rates. The net fixation rates in pmol cell^{-1} h^{-1} measured by membrane-inlet mass spectrometry by Schultz et al. (2007, their Fig. 3) were converted in pgC cell^{-1} day^{-1} considering 12 h of light. The organic carbon quota per cell was then calculated from the carbon uptake rate and the growth rate (their Table 1) using Eq. (5). The shift in metabolic rates and cell size for iron limitation was obtained from the difference between the iron-replete and iron-limited experiments.

Increase in pCO_2 in nitrate-limited conditions

The evolution in the metabolism–volume space following an increase in pCO_2 in nutrient-limited conditions is hard to assess. Ideally, when pCO_2 is changed in the chemostat, the dilution rate should be adjusted so that the nutrient concentration remains unaltered. In this way, two nutrient-limited chemostat experiments with different pCO_2 levels could be compared. To the best of my knowledge this has not been done. However, the results of Müller et al. (2012) suggest that the growth rate changes little with pCO_2 in conditions of nitrate limitation. In these experiments, the cell size and cell-specific photosynthesis rate of nitrate-limited cells increases with pCO_2. Nitrate is below the detection limit in all of these chemostat experiments. However, the extent to which the N / C ratio is lower in nitrate-depleted cells compared to nitrate-replete cells does not vary with pCO_2. Since decreased biomass N / C ratios are an indication of the extent of nitrate limitation, we can conclude that the level of limitation is similar in the nitrate-limited experiments. With this in mind, the behaviour of the cells in the Müller et al. (2012) experiment is comparable to that of the cell which experience a pCO_2 increase in optimum conditions: little or no change in the growth rate, an increase in the rate of photosynthesis and a decrease in calcification.

Appendix D: Limitations of the simple DEB approach

Proper DEB models of dividing unicellular organisms are more complex than the simple version introduced in Sect. 6. Specifically, (1) full DEB models include reserves, as well as structure and maturity, so that uptake and assimilation are decoupled and biomass stoichiometry varies with changes in nutrient availability (stoichiometry is fixed in the model used in this manuscript), (2) full DEB models consider the energy flow devoted to somatic maintenance and maturity maintenance, and (3) part of the energy rejected by the growth SU is re-absorbed into the reserves in full DEB models. Notwithstanding these limitations, the simple model presented in this manuscript has the minimum characteristics of DEB models that are necessary to reproduce typical covariations of metabolic rates and cell size.

The Supplement related to this article is available online at doi:10.5194/bg-12-4665-2015-supplement.

References

Arnold, H. E., Kerrison, P., and Steinke, M.: Interacting effects of ocean acidification and warming on growth and DMS-production in the haptophyte coccolithophoreEmiliania huxleyi, Glob. Change Biol., 19, 1007–1016, 2013.

Atkinson, D., Ciotti, B. J., and Montagnes, D. J. S.: Protists decrease in size linearly with temperature: ca. 2.5 % C-1, P. Roy. Soc. B, 270, 2605–2611, 2003.

Bach, L. T., Riebesell, U., and Georg Schulz, K.: Distinguishing between the effects of ocean acidification and ocean carbonation in the coccolithophore Emiliania huxleyi, Limnol. Oceanogr., 56, 2040–2050, 2011.

Bach, L. T., Bauke, C., Meier, K. J. S., Riebesell, U., and Schulz, K. G.: Influence of changing carbonate chemistry on morphology and weight of coccoliths formed by Emiliania huxleyi, Biogeosciences, 9, 3449–3463, doi:10.5194/bg-9-3449-2012, 2012.

Bach, L. T., Riebesell, U., Gutowska, M. A., Federwisch, L., and Schulz, K. G.: A unifying concept of coccolithophore sensitivity to changing carbonate chemistry embedded in an ecological framework, Prog. Oceanogr., 135, 125–138, 2015.

Banavar, J. R., Damuth, J., Maritan, A., and Rinaldo, A.: Supply-demand balance and metabolic scaling, P. Natl. Acad. Sci., 99, 10506–10509, 2002.

Beaufort, L., Couapel, M., Buchet, N., Claustre, H., and Goyet, C.: Calcite production by coccolithophores in the south east Pacific Ocean, Biogeosciences, 5, 1101–1117, doi:10.5194/bg-5-1101-2008, 2008.

Beaufort, L., Probert, I., de Garidel-Thoron, T., Bendif, E. M., Ruiz-Pino, D., Metzl, N., Goyet, C., Buchet, N., Coupel, P., Grelaud, M., Rost, B., Rickaby, R. E. M., and de Vargas, C.: Sensitivity of coccolithophores to carbonate chemistry and ocean acidification, Nature, 476, 80–83, 2011.

Behrenfeld, M. J., O'Malley, R. T., Siegel, D. A., McClain, C. R., Sarmiento, J. L., Feldman, G. C., Milligan, A. J., Falkowski, P. G., Letelier, R. M., and Boss, E. S.: Climate-driven trends in contemporary ocean productivity, Nature, 444, 752–755, 2006.

Berger, C., Meier, K. J. S., Kinkel, H., and Baumann, K.-H.: Changes in calcification of coccoliths under stable atmospheric CO2, Biogeosciences, 11, 929–944, doi:10.5194/bg-11-929-2014, 2014.

Bollmann, J. and Herrle, J. O.: Morphological variation of Emiliania huxleyi and sea surface salinity, Earth Planet. Sci. Lett., 255, 273–288, 2007.

Bolton, C. T. and Stoll, H. M.: Late Miocene threshold response of marine algae to carbon dioxide limitation, Nature, 500, 558–562, 2013.

Bopp, L.: Response of diatoms distribution to global warming and potential implications: A global model study, Geophys. Res. Lett., 32, L19606, doi:10.1029/2005GL023653, 2005.

Bopp, L., Monfray, P., Aumont, O., Dufresne, J.-L., Le Treut, H., Madec, G., Terray, L., and Orr, J. C.: Potential impact of climate change on marine export production, Glob. Biogeochem. Cycle, 15, 81–99, 2001.

Borchard, C., Borges, A. V., Händel, N., and Engel, A.: Biogeochemical response of Emiliania huxleyi (PML B92/11) to elevated CO2 and temperature under phosphorous limitation: A chemostat study, J. Exp. Mar. Biol. Ecol., 410, 61–71, 2011.

Broecker, W. and Clark, E.: Ratio of coccolith CaCO(1) to foraminifera CaCO(1) in late Holocene deep sea sediments, Paleoceanography, 24, PA3205, doi:10.1029/2009PA001731, 2009.

Brownlee, C., Davis, M., Nimer, N., Dong, L. F., and Merret, M. J.: Calcification, photosynthesis and intracellular regulation of Emiliania huxleyi, Bulletin de l'Institut Océanographique de Monaco, 14, 19–35, 1995.

Cermeño, P., Marañón, E., Harbour, D., and Harris, R. P.: Invariant scaling of phytoplankton abundance and cell size in contrasting marine environments, Ecol. Lett., 9, 1210–1215, 2006.

Cook, S. S., Whittock, L., Wright, S. W., and Hallegraeff, G. M.: Photosynthetic pigment and genetic differences between two southern ocean morphotypes of emiliania huxleyi (haptophyta), J. Phycol., 47, 615–626, 2011.

Cubillos, J. C., Wright, S. W., Nash, G., de Salas, M. F., Griffiths, B., Tilbrook, B., Poisson, A., and Hallegraeff, G. M.: Calcification morphotypes of the coccolithophorid Emiliania huxleyi in the Southern Ocean: changes in 2001 to 2006 compared to historical data, Mar. Ecol.-Prog. Ser., 348, 47–54, 2007.

De Bodt, C., Van Oostende, N., Harlay, J., Sabbe, K., and Chou, L.: Individual and interacting effects of pCO2 and temperature on *Emiliania huxleyi* calcification: study of the calcite production, the coccolith morphology and the coccosphere size, Biogeosciences, 7, 1401–1412, doi:10.5194/bg-7-1401-2010, 2010.

Feng, Y., Warner, M. E., Zhang, Y., Sun, J., Fu, F.-X., Rose, J. M., and Hutchins, D. A.: Interactive effects of increased pCO2, temperature and irradiance on the marine coccolithophore *Emiliania huxleyi* (Prymnesiophyceae), European J. Phycol., 43, 87–98, 2008.

Fiorini, S., Middelburg, J. J., and Gattuso, J.-P.: Testing the Effects of Elevated pCO2 on Coccolithophores (Prymnesiophyceae): Comparison between Haploid and Diploid Life Stages1, J. Phycol., 47, 1281–1291, 2011.

Gehlen, M., Gangstø, R., Schneider, B., Bopp, L., Aumont, O., and Ethe, C.: The fate of pelagic CaCO3 production in a high CO2 ocean: a model study, Biogeosciences, 4, 505–519, doi:10.5194/bg-4-505-2007, 2007.

Geider, R. and La Roche, J.: Redfield revisited: variability of C : N : P in marine microalgae and its biochemical basis, Eur. J. Phycol., 37, 1–17, 2002.

Grelaud, M., Schimmelmann, A., and Beaufort, L.: Coccolithophore response to climate and surface hydrography in Santa

Barbara Basin, California, AD 1917–2004, Biogeosciences, 6, 2025–2039, doi:10.5194/bg-6-2025-2009, 2009.

Hagino, K., Okada, H., and Matsuoka, H.: Coccolithophore assemblages and morphotypes of Emiliania huxleyi in the boundary zone between the cold Oyashio and warm Kuroshio currents off the coast of Japan, Mar. Micropaleontol., 55, 19–47, 2005.

Henderiks, J.: Coccolithophore size rules – Reconstructing ancient cell geometry and cellular calcite quota from fossil coccoliths, Mar. Micropaleontol., 67, 143–154, 2008.

Henderiks, J., Winter, A., Elbrächter, M., Feistel, R., der Plas, A., Nausch, G., and Barlow, R.: Environmental controls on Emiliania huxleyi morphotypes in the Benguela coastal upwelling system (SE Atlantic), Mar. Ecol.-Prog. Ser., 448, 51–66, 2012.

Honjo, S., Manganini, S. J., Krishfield, R. A., and Francois, R.: Particulate organic carbon fluxes to the ocean interior and factors controlling the biological pump: A synthesis of global sediment trap programs since 1983, Prog. Oceanogr., 76, 217–285, 2008.

Hoppe, C. J. M., Langer, G., and Rost, B.: Emiliania huxleyi shows identical responses to elevated pCO$_2$ in TA and DIC manipulations, J. Exp. Mar. Biol. Ecol., 406, 54–62, 2011.

Horigome, M. T., Ziveri, P., Grelaud, M., Baumann, K.-H., Marino, G., and Mortyn, P. G.: Environmental controls on the Emiliania huxleyi calcite mass, Biogeosciences, 11, 2295–2308, doi:10.5194/bg-11-2295-2014, 2014.

Huete-Ortega, M., Cermeno, P., Calvo-Diaz, A., and Marañón, E.: Isometric size-scaling of metabolic rate and the size abundance distribution of phytoplankton, P. Roy. Soc. B, 279, 1815–1823, 2012.

Iglesias-Rodríguez, D. M., Schofield, O. M., Batley, J., Medlin, L. K., and Hayes, P. K.: Intraspecific genetic diversity in the marine coccolithophore emiliania huxleyi (prymnesiophyceae): the use of microsatellite analysis in marine phytoplankton population studies1, J. Phycol., 42, 526–536, 2006.

Iglesias-Rodríguez, M. D.: Representing key phytoplankton functional groups in ocean carbon cycle models: Coccolithophorids, Glob. Biogeochem. Cycle, 16, 1100, doi:10.1029/2001GB001454, 2002.

Iglesias-Rodriguez, M. D., Halloran, P. R., Rickaby, R. E. M., Hall, I. R., Colmenero-Hidalgo, E., Gittins, J. R., Green, D. R. H., Tyrrell, T., Gibbs, S. J., von Dassow, P., Rehm, E., Armbrust, E. V., and Boessenkool, K. P.: Phytoplankton calcification in a high-CO$_2$ world, Science, 320, 336–340, 2008.

Kaffes, A., Thoms, S., Trimborn, S., Rost, B., Langer, G., Richter, K.-U., Köhler, A., Norici, A., and Giordano, M.: Carbon and nitrogen fluxes in the marine coccolithophore Emiliania huxleyi grown under different nitrate concentrations, J. Exp. Mar. Biol. Ecol., 393, 1–8, 2010.

Kooijman, S. A. L. M.: Dynamic Energy Budget Theory for Metabolic Organisation, Cambridge University Press, Cambridge, 532 pp., 2010.

Krug, S. A., Schulz, K. G., and Riebesell, U.: Effects of changes in carbonate chemistry speciation on Coccolithus braarudii: a discussion of coccolithophorid sensitivities, Biogeosciences, 8, 771–777, doi:10.5194/bg-8-771-2011, 2011.

Langer, G., Geisen, M., Baumann, K. H., Klas, J., Riebesell, U., Thoms, S., and Young, J. R.: Species-specific responses of calcifying algae to changing seawater carbonate chemistry, Geochem. Geophys. Geosyst., 7, Q09006, doi:10.1029/2005GC001227, 2006.

Langer, G., Nehrke, G., Probert, I., Ly, J., and Ziveri, P.: Strain-specific responses of Emiliania huxleyi to changing seawater carbonate chemistry, Biogeosciences, 6, 2637–2646, doi:10.5194/bg-6-2637-2009, 2009.

Langer, G., Oetjen, K., and Brenneis, T.: Calcification of Calcidiscus leptoporus under nitrogen and phosphorus limitation, J. Exp. Mar. Biol. Ecol., 413, 131–137, 2012.

Langer, G., Oetjen, K., and Brenneis, T.: Coccolithophores do not increase particulate carbon production under nutrient limitation: A case study using Emiliania huxleyi (PML B92/11), J. Exp. Mar. Biol. Ecol., 443, 155–161, 2013.

LaRoche, J., Rost, B., and Engel, A.: Bioassays, batch culture and chemostat experimentation, in: Guide of best practices for ocean acidification research and data processing, edited by: Riebesell, U., Fabry, V. J., Hansson, L., and Gattuso, J.-P., Publications office of the European Union, Luxembourg, 2010.

Laws, E. A. and Bannister, T. T.: Nutrient-Limited and Light-Limited Growth of Thalassiosira-Fluviatilis in Continuous Culture, with Implications for Phytoplankton Growth in the Ocean, Limnol. Oceanogr., 25, 457–473, 1980.

Lee, K., Tong, L. T., Millero, F. J., Sabine, C. L., Dickson, A. G., Goyet, C., Park, G.-H., Wanninkhof, R., Feely, R. A., and Key, R. M.: Global relationships of total alkalinity with salinity and temperature in surface waters of the world's oceans, Geophys. Res. Lett., 33, L19605, doi:10.1029/2006GL027207, 2006.

Lefebvre, S. C., Benner, I., Stillman, J. H., Parker, A. E., Drake, M. K., Rossignol, P. E., Okimura, K. M., Komada, T., and Carpenter, E. J.: Nitrogen source and pCO2 synergistically affect carbon allocation, growth and morphology of the coccolithophore Emiliania huxleyi: potential implications of ocean acidification for the carbon cycle, Glob. Change Biol., 18, 493–503, 2011.

Linschooten, C., Vanbleijswijk, J. D. L., Vanemburg, P. R., Devrind, J. P. M., Kempers, E. S., Westbroek, P., and Devrinddejong, E. W.: Role of the Light-Dark Cycle and Medium Composition on the Production of Coccoliths by Emiliania-Huxleyi (Haptophyceae), J. Phycol., 27, 82–86, 1991.

Lohbeck, K. T., Riebesell, U., and Reusch, T. B. H.: Adaptive evolution of a key phytoplankton species to ocean acidification, Nat. Geosci., 5, 346–351, 2012.

López-Sandoval, D. C., Rodríguez-Ramos, T., Cermeño, P., Sobrino, C., and Marañón, E.: Photosynthesis and respiration in marine phytoplankton: Relationship with cell size, taxonomic affiliation, and growth phase, J. Exp. Mar. Biol. Ecol., 457, 151–159, 2014.

Lopez-Urrutia, A., San Martin, E., Harris, R.P. and Irigoien, X.: Scaling the metabolic balance of the oceans, P. Natl. Acad. Sci., 103, 8739–8744, 2006.

Lorena, A., Marques, G. M., Kooijman, S. A. L. M., and Sousa, T.: Stylized facts in microalgal growth: interpretation in a dynamic energy budget context, Philos. T. R. Soc. B, 365, 3509–3521, 2010.

Marañón, E.: Inter-specific scaling of phytoplankton production and cell size in the field, J. Plankton Res., 30, 157–163, 2008.

Marañón, E., Cermeño, P., Rodriguez, J., Zubkov, M. V., and Harris, R. P.: Scaling of phytoplankton photosynthesis and cell size in the ocean, Limnol. Oceanogr., 52, 2190–2198, 2007.

Marañón, E., Cermeño, P., López-Sandoval, D. C., Rodríguez-Ramos, T., Sobrino, C., Huete-Ortega, M., Blanco, J. M., Rodríguez, J., and Fussmann, G.: Unimodal size scaling of phyto-

plankton growth and the size dependence of nutrient uptake and use, Ecol. Lett., 16, 371–379, 2013.

Medlin, L. K., Barker, G. L. A., Campbell, L., Green, J. C., Hayes, P. K., Marie, D., Wrieden, S., and Vaulot, D.: Genetic characterisation of Emiliania huxleyi (Haptophyta), J. Mar. Sys., 9, 13–31, 1996.

Meier, K. J. S., Beaufort, L., Heussner, S., and Ziveri, P.: The role of ocean acidification in *Emiliania huxleyi* coccolith thinning in the Mediterranean Sea, Biogeosciences, 11, 2857–2869, doi:10.5194/bg-11-2857-2014, 2014.

Menden-Deuer, S. and Lessard, E. J.: Carbon to volume relationships for Dinoflagellates, Diatoms, and other protist plankton, Limnol. Oceanogr., 45, 569–579, 2000.

Mitrovic, S. M., Howden, C. G., and Bowling, L. C.: Unusual allometry between in situ growth of freshwater phytoplancton under static and fluctuating light environments: possible implications for dominance, J. Plankton Res., 25, 517–526, 2005.

Montagnes, D. J. S., Berges, J. A., Harrison, P. J., and Taylor, F. J. R.: Estimating Carbon, Nitrogen, Protein, and Chlorophyll *a* from Volume in Marine-Phytoplankton, Limnol. Oceanogr., 39, 1044–1060, 1994.

Muller, E. B., Ananthasubramaniam, B., Klanjšček, T., and Nisbet, R. M.: Entrainment of cell division in phytoplankton with dynamic energy budgets, J. Sea Res., 66, 447–455, 2011.

Muller, E. B. and Nisbet, R. M.: Dynamic energy budget modeling reveals the potential of future growth and calcification for the coccolithophoreEmiliania huxleyiin an acidified ocean, Glob. Change Biol., 20, 2031–2038, 2014.

Muller, M. N., Antia, A. N., and LaRoche, J.: Influence of cell cycle phase on calcification in the coccolithophore *Emiliania huxleyi*, Limnol. Oceanogr., 53, 506–512, 2008.

Müller, M. N., Beaufort, L., Bernard, O., Pedrotti, M. L., Talec, A., and Sciandra, A.: Influence of CO_2 and nitrogen limitation on the coccolith volume of Emiliania huxleyi (Haptophyta), Biogeosciences, 9, 4155–4167, doi:10.5194/bg-9-4155-2012, 2012.

Muller, P. J., Suess, E., and Ungerer, C. A.: Amino-Acids and Amino-Sugars of Surface Particulate and Sediment Trap Material from Waters of the Scotia Sea, Deep-Sea Res., 33, 819–838, 1986.

Niklas, K. J. and Enquist, B. J.: Invariant scaling relationships for interspecific plant biomass production rates and body size, P. Natl. Acad. Sci., 98, 2922–2927, 2001.

Oviedo, A. M., Langer, G., and Ziveri, P.: Effect of phosphorus limitation on coccolith morphology and element ratios in Mediterranean strains of the coccolithophore Emiliania huxleyi, J. Exp. Mar. Biol. Ecol., 459, 105–113, 2014.

Paasche, E.: Marine plankton algae grown with light-dark cycles. I. Coccolithus huxlei, Physiol. Plantarum, 20, 946–956, 1967.

Paasche, E.: Reduced coccolith calcite production under light-limited growth: a comparative study of three clones of *Emiliania huxleyi* (Prymnesiophyceae), Phycologia, 38, 508–516, 1999.

Paasche, E.: A review of the coccolithophorid Emiliania huxleyi (Prymnesiophyceae), with particular reference to growth, coccolith formation, and calcification-photosynthesis interactions, Phycologia, 40, 503–529, 2001.

Paasche, E., Brubak, S., Skattebol, S., Young, J. R., and Green, J. C.: Growth and calcification in the coccolithophorid Emiliania huxleyi (Haptophyceae) at low salinities, Phycologia, 35, 394–403, 1996.

Poulton, A. J., Adey, T. R., Balch, W. M., and Holligan, P. M.: Relating coccolithophore calcification rates to phytoplankton community dynamics: Regional differences and implications for carbon export, Deep-Sea Res. Pt. II, 54, 538–557, 2007.

Poulton, A. J., Young, J. R., Bates, N. R., and Balch, W. M.: Biometry of detached Emiliania huxleyi coccoliths along the Patagonian Shelf, Mar. Ecol.-Prog. Ser., 443, 1–17, 2011.

Poulton, A. J., Stinchcombe, M. C., Achterberg, E. P., Bakker, D. C. E., Dumousseaud, C., Lawson, H. E., Lee, G. A., Richier, S., Suggett, D. J., and Young, J. R.: Coccolithophores on the northwest European shelf: calcification rates and environmental controls, Biogeosciences, 11, 3919–3940, doi:10.5194/bg-11-3919-2014, 2014.

Powell, E. O.: Growth rate and generation time of bacteria, with special reference to continuous culture, J. Gen. Microbiol., 15, 492–511, 1956.

Raven, J. A.: The twelfth Tansley Lecture, Small is beautiful: the picophytoplankton, Functional Ecology, 12, 503–513, 1998.

Raven, J. A. and Crawfurd, K.: Environmental controls on coccolithophore calcification, Mar. Ecol.-Prog. Ser., 470, 137–166, 2012.

Read, B. A., Kegel, J., Klute, M. J., Kuo, A., Lefebvre, S. C., Maumus, F., Mayer, C., Miller, J., Monier, A., Salamov, A., Young, J., Aguilar, M., Claverie, J.-M., Frickenhaus, S., Gonzalez, K., Herman, E. K., Lin, Y.-C., Napier, J., Ogata, H., Sarno, A. F., Shmutz, J., Schroeder, D., de Vargas, C., Verret, F., von Dassow, P., Valentin, K., Van de Peer, Y., Wheeler, G., Dacks, J. B., Delwiche, C. F., Dyhrman, S. T., Gloeckner, G., John, U., Richards, T., Worden, A. Z., Zhang, X., Grigoriev, I. V., Allen, A. E., Bidle, K., Borodovsky, M., Bowler, C., Brownlee, C., Cock, J. M., Elias, M., Gladyshev, V. N., Groth, M., Guda, C., Hadaegh, A., Iglesias-Rodriguez, M. D., Jenkins, J., Jones, B. M., Lawson, T., Leese, F., Lindquist, E., Lobanov, A., Lomsadze, A., Malik, S.-B., Marsh, M. E., Mackinder, L., Mock, T., Mueller-Roeber, B., Pagarete, A., Parker, M., Probert, I., Quesneville, H., Raines, C., Rensing, S. A., Riano-Pachon, D. M., Richier, S., Rokitta, S., Shiraiwa, Y., Soanes, D. M., van der Giezen, M., Wahlund, T. M., Williams, B., Wilson, W., Wolfe, G., Wurch, L. L., and Emiliania Huxleyi, A.: Pan genome of the phytoplankton Emiliania underpins its global distribution, Nature, 499, 209–213, 2013.

Reinfelder, J. R.: Carbon Concentrating Mechanisms in Eukaryotic Marine Phytoplankton, Annu. Rev. Mar. Sci., 3, 291–315, 2011.

Riebesell, U., Zondervan, I., Rost, B., Tortell, P. D., Zeebe, R. E., and Morel, F. M. M.: Reduced calcification of marine plankton in response to increased atmospheric CO_2, Nature, 407, 364–367, 2000.

Riegman, R., Stolte, W., Noordeloos, A. A. M., and Slezak, D.: Nutrient uptake, and alkaline phosphate (EC 3 : 1 : 3 : 1) activity of Emiliania huxleyi (Prymnesiophyceae) during growth under N and P limitation in continuous cultures, J. Phycol., 36, 87–96, 2000.

Rokitta, S. D. and Rost, B.: Effects of CO_2 and their modulation by light in the life-cycle stages of the coccolithophore Emiliania huxleyi, Limnol. Oceanogr., 57, 607–618, 2012.

Rost, B., Zondervan, I., and Riebesell, U.: Light-dependent carbon isotope fractionation in the coccolithophorid Emiliania huxleyi, Limnol. Oceanogr., 47, 120–128, 2002.

Rost, B., Riebesell, U., Burkhardt, S., and Sultemeyer, D.: Carbon acquisition of bloom-forming marine phytoplankton, Limnol. Oceanogr., 48, 55–67, 2003.

Rouco, M., Branson, O., Lebrato, M., and Iglesias-Rodríguez, M. D.: The effect of nitrate and phosphate availability on Emiliania huxleyi (NZEH) physiology under different CO_2 scenarios, Front. Microbiol., 4, 155, doi:10.3389/fmicb.2013.00155, 2013.

Satoh, M., Iwamoto, K., Suzuki, I., and Shiraiwa, Y.: Cold Stress Stimulates Intracellular Calcification by the Coccolithophore, Emiliania huxleyi (Haptophyceae) Under Phosphate-Deficient Conditions, Mar. Biotechnol., 11, 327–333, 2008.

Schiebel, R., Brupbacher, U., Schmidtko, S., Nausch, G., Waniek, J. J., and Thierstein, H.-R.: Spring coccolithophore production and dispersion in the temperate eastern North Atlantic Ocean, J. Geophys. Res., 116, 116, doi:10.1029/2010JC006841, 2011.

Schlüter, L., Lohbeck, K. T., Gutowska, M. A., Gröger, J. P., Riebesell, U., and Reusch, T. B. H.: Adaptation of a globally important coccolithophore to ocean warming and acidification, Nature Climate Change, 4, 1024–1030, 2014.

Schroeder, D. C., Biggi, G. F., Hall, M., Davy, J., Martínez, J. M., Richardson, A. J., Malin, G., and Wilson, W. H.: A genetic marker to separate emiliania huxleyi (prymnesiophyceae) morphotypes, J. Phycol., 41, 874–879, 2005.

Schulz, K. G., Rost, B., Burkhardt, S., Riebesell, U., Thoms, S., and Wolf-Gladrow, D. A.: The effect of iron availability on the regulation of inorganic carbon acquisition in the coccolithophore Emiliania huxleyi and the significance of cellular compartmentation for stable carbon isotope fractionation, Geochim. Cosmochim. Ac., 71, 5301–5312, 2007.

Sciandra, A., Harlay, J., Lefevre, D., Lemee, R., Rimmelin, P., Denis, M., and Gattuso, J. P.: Response of coccolithophorid Emiliania huxleyi to elevated partial pressure of CO_2 under nitrogen limitation, Mar. Ecol.-Prog. Ser., 261, 111–122, 2003.

Sett, S., Bach, L. T., Schulz, K. G., Koch-Klavsen, S., Lebrato, M., and Riebesell, U.: Temperature Modulates Coccolithophorid Sensitivity of Growth, Photosynthesis and Calcification to Increasing Seawater pCO_2$, PLoS ONE, 9, e88308, doi:10.1371/journal.pone.0088308, 2014.

Shutler, J. D., Land, P. E., Brown, C. W., Findlay, H. S., Donlon, C. J., Medland, M., Snooke, R., and Blackford, J. C.: Coccolithophore surface distributions in the North Atlantic and their modulation of the air-sea flux of CO_2 from 10 years of satellite Earth observation data, Biogeosciences, 10, 2699–2709, doi:10.5194/bg-10-2699-2013, 2013.

Smith, H. E. K., Tyrrell, T., Charalampopoulou, A., Dumousseaud, C., Legge, O. J., Birchenough, S., Pettit, L. R., Garley, R., Hartman, S. E., Hartman, M. C., Sagoo, N., Daniels, C. J., Achterberg, E. P., and Hydes, D. J.: Predominance of heavily calcified coccolithophores at low $CaCO_3$ saturation during winter in the Bay of Biscay, P. Natl. Acad. Sci., 109, 8845–8849, 2012.

Stolte, W., McCollin, T., and Noordeloos, A. M.: Effect of nitrogen source on the size distribution within marine phytoplankton populations, J. Exp. Mar. Biol. Ecol., 184, 83–97, 1994.

Takahashi, T.: Climatological mean and decadal change in surface ocean pCO2, and net sea–air CO_2 flux over the global oceans, Deep-Sea Res. Pt. II, 56, 554–577, 2009.

Thomas, M. K., Kremer, C. T., Klausmeier, C. A., and Litchman, E.: A global pattern of thermazl adaptation in marine phytoplankton, Science, 338, 1085–1088, 2012.

Trimborn, S., Langer, G., and Rost, B.: Effect of varying calcium concentrations and light intensities on calcification and photosynthesis in Emiliania huxleyi, Limnol. Oceanogr., 52, 2285–2293, 2007.

van Rijssel, M. and Gieskes, W. W. C.: Temperature, light, and the dimethylsulfoniopropionate (DMSP) content of Emiliania huxleyi (Prymnesiophyceae), J. Sea Res., 48, 17–27, 2002.

Vanbleijswijk, J. D. L., Kempers, R. S., Veldhuis, M. J., and Westbroek, P.: Cell and Growth-Characteristics of Type-a and Type-B of Emiliania-Huxleyi (Prymnesiophyceae) as Determined by Flow-Cytometry and Chemical-Analyses, J. Phycol., 30, 230–241, 1994.

Walsby, A. F. and Reynolds, C. S.: Sinking and floating. In: The physiological ecology of phytoplankton, Morris, I. (Ed.), University of California Press, Berkeley, 371–412, 1980.

West, G. B., Brown, J. H., and Enquist, B. J.: A general model for the origin of allometric scaling laws in biology, Science, 276, 122–126, 1997.

Wilson, J. D., Barker, S., and Ridgwell, A.: Assessment of the spatial variability in particulate organic matter and mineral sinking fluxes in the ocean interior: Implications for the ballast hypothesis, Glob. Biogeochem. Cycle, 26, GB4011, doi:10.1029/2012GB004398, 2012.

Winter, A., Henderiks, J., Beaufort, L., Rickaby, R. E. M., and Brown, C. W.: Poleward expansion of the coccolithophore Emiliania huxleyi, J. Plankton Res., 36, 316–325, 2013.

Young, J. R. and Henriksen, K.: Biomineralization within vesicles: The calcite of coccoliths, Biomineralization, 54, 189–215, 2003.

Young, J. R. and Westbroek, P.: Genotypic variation in the coccolitophorid species *Emiliania huxleyi*, Mar. Micropaleontol., 18, 5–23, 1991.

Young, J. R., Poulton, A. J., and Tyrrell, T.: Morphology of *Emiliania huxleyi* coccoliths on the northwestern European shelf – is there an influence of carbonate chemistry?, Biogeosciences, 11, 4771–4782, doi:10.5194/bg-11-4771-2014, 2014.

Zondervan, I.: The effects of light, macronutrients, trace metals and CO2 on the production of calcium carbonate and organic carbon in coccolithophores - A review, Deep-Sea Res. Part II, 54, 521–537, 2007.

Zondervan, I., Rost, B., and Riebesell, U.: Effect of CO_2 concentration on the PIC/POC ratio in the coccolithophore *Emiliania huxleyi* grown under light-limiting conditions and different daylengths, J. Exp. Mar. Biol. Ecol., 272, 55–70, 2002.